UNIVERSIDADE D
COIMBRA

Guilherme Nuno Mendes Veríssimo

WATER JET MODELLING AND CHARACTERIZATION

APPLICATION IN FIREFIGHTING TECHNOLOGIES

VOLUME 1

Dissertação no âmbito do Mestrado Integrado em Engenharia Mecânica orientada pelo Professor Doutor Carlos Xavier Pais Viegas e apresentada ao Departamento de Engenharia Mecânica da Universidade de Coimbra

Setembro de 2019

1 2 9 0

FACULDADE DE CIÊNCIAS E TECNOLOGIA
UNIVERSIDADE D COIMBRA

Water jet modelling and characterization for application in firefighting technologies

Submitted in Partial Fulfilment of the Requirements for the Degree of Master in Mechanical Engineering in the speciality of Production and Project

Modelação e caracterização de jatos de água para aplicação em tecnologias de combate a incêndios

Author

Guilherme Nuno Mendes Veríssimo

Advisors

Carlos Xavier Pais Viegas

Domingos Xavier Filomeno Carlos Viegas

Jury

President	**Professor Doutor Jorge Campos da Silva André** **Professor da Universidade de Coimbra**
Vowel	**Professor Doutor Gilberto Cordeiro Vaz** **Professor Adjunto do Instituto Politécnico de Coimbra**
Advisor	**Professor Doutor Carlos Xavier Pais Viegas** **Professor Auxiliar da Universidade de Coimbra**

Coimbra, September, 2019

ACKNOWLEDGEMENTS

Reported study occurred due to collaboration among ADAI's researchers. Their support was fundamental to execute the experimental investigation. Particularly, my advisor Professor Carlos Viegas. The author acknowledges as well extremely helpful discussions with Professor Adrian Peidro in order to implement the theoretical model. Also, family, friends and Andreia for all the emotional support.

Abstract

Annually, in Mediterranean countries, wildfires origin patrimonial losses, injured people or life losses. To address the mentioned problem, ADAI's researchers are projecting two firefighting systems: 1) a portable water monitor capable of detecting and directing a waterjet to a heat source, and 2) a drone with an attached nozzle and water hose, with the purpose of fighting wildfires from the air. Both devices labor using large water flows and large service pressures. A careful design and project are required, since this results in large reaction forces.

The water jet kickback force's problematic has only a few addressed bibliographies, so any contribution to this topic will be invaluable to further progress knowledge and the state-of-the-art.

By above-mentioned reasons, the main objective of the work presented is the characterization and modelling of a water jet, focusing principally on the nozzle reactions and the variables that affect it, like hose tension, pump's output flow, within others. The intention is to use the collected information in the design of the two referred firefighting technologies.

The method adopted, consists in directly measuring nozzle reactions in a real-life situation, consequently, the achieved results are the true reactions that a fireman should feel while fighting a wildfire. Those results disagree with part of the addressed literature and concede us the opportunity to conclude that the forces acting on the hose and their reactions while contacting with the ground are essential to comprehend nozzle reaction.

Keywords modelling, waterjet, firefighting technologies, drone, water monitor, nozzle reactions.

Resumo

Anualmente, nos países de clima mediterrâneo, os incêndios causam inúmeros ferimentos, tanto na população civil, como nos bombeiros, para além da incontável perda de património.

Com vista a combater o problema mencionado, os investigadores da ADAI projetaram dois sistemas de combate a incêndios. Um deles, um drone para combater fogos pelo meio aéreo, outro, uma agulheta portante, capaz de detetar e direcionar um jato de água para uma fonte de calor. Ambos trabalham com grandes caudais de água conjugados com grandes pressões de serviço, o que resulta em grandes forças de reação do jato, e por esta razão, os dois sistemas têm de ser projetos de maneira cuidadosa.

Visto que é uma problemática com pobre bibliografia associada, qualquer contribuição para este assunto será importante para progredir no conhecimento e aumentar o estado-de-arte.

Pelas razões apresentadas, o objetivo do trabalho desenvolvido é a caracterização e modelação de jatos de água, focando principalmente nas reações da agulheta e nas varáveis que as afetam, tal como a tensão da mangueira, caudal ejetado, entre outras. A intenção é aplicar a informação recolhida nas duas aplicações de combate a incêndios atrás referidas.

O método adotado, consistiu em medir, diretamente, as reações numa agulheta durante uma situação semelhante com uma de vida real, consequentemente, os resultados extraídos são as reações que um bombeiro deve sentir, tal como as que os dois sistemas referidos vão terão que suportar em serviço. Os resultados atingidos discordam de parte das investigações realizadas sobre o assunto, permitiram-nos, também, observar que as forças exercidas pela mangueira (e as suas reações em contacto com o terreno) são essências para compreender as forças exercidas numa agulheta debitando um jato de água.

Palavras-chave: Jato de água, modelação, tecnologias de combate ao fogo, drone, agulheta portante, forças numa agulheta.

Contents

LIST OF FIGURES

LIST OF TABLES

LIST OF ACRONYMS/ ABBREVIATIONS

Acronyms/Abbreviations

ADAI – Associação para o Desenvolvimento de Aerodinâmica Industrial

NFPA – National Fire Protection Association

UAV – Unmanned Aerial Vehicle

1. INTRODUCTION

1.1. Motivation

Mediterranean countries' summer weather, whom comprehend high temperatures and low humidity, combined with large fuel accumulation along the forest territory, generate perfect conditions to originate large wildfires, figure (1.1) displays the large number of occurrences among South European's countries between 2012 and 2016[1].

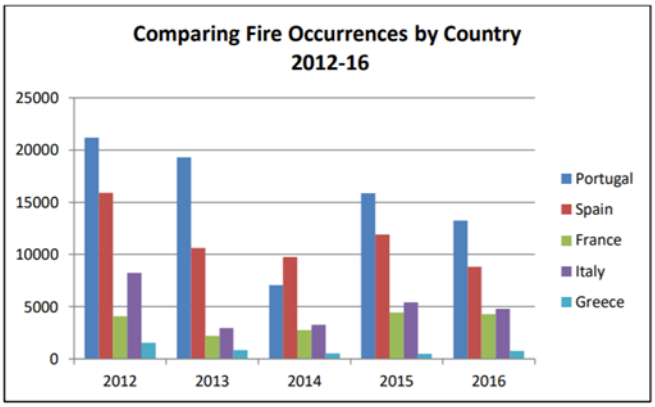

Figure 1.1 - Fire Occurrences in South European countries between 2012 and 2016[1]

Every year, the population in such countries suffers patrimonial losses, firemen suffer injuries and a large part of the forest territory is lost. As demonstrated by figure (1.2) that displays the large number of hectares burned in Portugal's Centro Region between 2001 and 2017[1]. Having into account that Centro Region contains near 2,850,000 hectares, complementing forest and urban areas, thus, exclusively in 2017 a fifth of the total area was burned.

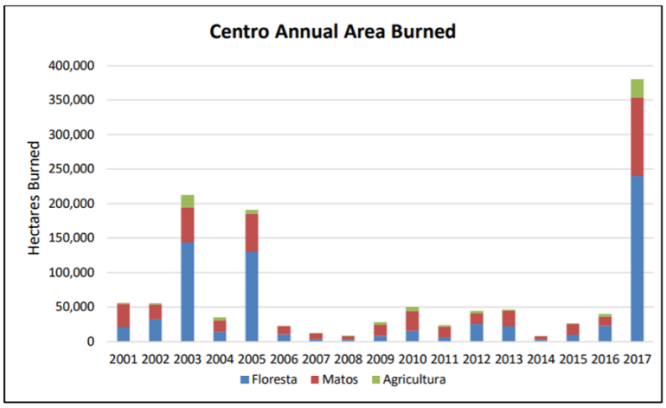

Figure 1.2 - Number of hectares burned in Portugal Centro Region between 2001 and 2017

However, this problem's worst consequence is the loss of lives to wildfires, as happened in Pedrógão Grande 2017 tragedy. Towards exemplify the tragedy's scale, the resultant numbers are displayed in figure 1.3 [2]:

Toll of the Pedrógão Grande fire

- 66 people killed, many of them trapped in vehicles on the N-236 road
- 253 injured
- 485 houses destroyed
- 53,000 hectares of land burned, including 20,000 hectares of forest
- 2,018 farmers affected at a cost of €21m (£19m; $25m)
- 49 companies affected at a cost of €31m

Figure 1.3 - Toll of the Pedrógão Grande wildfire

To address this issue, ADAI's researchers are developing two systems to support firefighters (figure 1.4): 1) a portable water monitor capable of detecting and directing a waterjet to a heat source, and 2) a drone with an attached nozzle and water hose, with the purpose of fighting wildfires from the air. These two systems' development is financed by the European financial fund Portugal 2020.

Figure 1.4 - Two referred firefighting technologies; 1) on the left the portable water monitor; 2) on the right, the drone

Both devices use large water flows at large pressures. A careful design and project are required, since this results in large reaction forces, which must be supported by the devices. In the case of a small, light and portable device such as the water monitor, or a light flying unmanned air vehicle, such as the drone, this becomes even more pertinent. This work's main goal is the, complete waterjet reaction forces characterization and modelling, particularly nozzle reaction. Nozzle reaction (or kickback) is the force exerted by a stationary nozzle supplied by a flexible hose, on a firefighter (or any other anchor)[3].

Regarding the drone application (figure 1.5), is simple to comprehend that the reactions on all axis are important to analyze for two main reasons: First, the preferential axis for the drone to exert force is the vertical axis, which is the axis of the propulsion force of its propellers. Forces and moment in any other axis, force the drone to change its pitch and roll angles from the horizontal state, thus loosing lift. While modern UAV controllers quickly overcome and compensate punctual disturbances and forces, one can still optimize and design the water nozzle mechanism in a way that reduces as much as possible the moment and forces on the horizontal plane, thus increasing the propulsion system efficiency of the drone. The second reason has to do with the hose pulling and deformation, which in turn causes further forces and moment on the water nozzle, according to the geometry of the hose. This effect must be thoroughly analyzed to better design the hose support or optimize the drone movement and path planning, in order to minimize the hose bending.

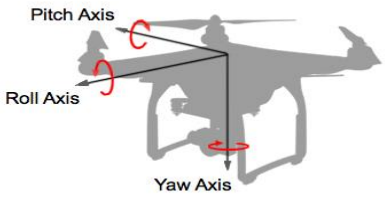

Figure 1.5 - Drone axes and rotations[4]

Regarding the water monitor application (figure 1.6): in this case the forces on the vertical axis are not critical since the equipment is placed on the ground, so the equipment own weight restrains the movement on this axis. On the other hand, the moment is important so that the equipment remains fixed in place and does not rotate on its own axis when changing the yaw angle of the nozzle or does not topple over due to the moment in the horizontal axes. To avoid this, one must know the magnitude of the forces and moment involved and design the mechanism base accordingly.

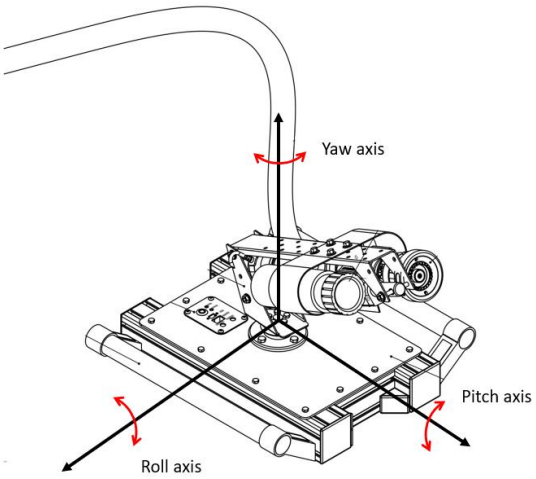

Figure 1.6 - Water monitor axes and rotations

The results of this research can then be used to optimize the water monitor design and actuators, as well as the drone propulsion system. Furthermore, they can also be useful for further applications, such as water propelled device. Large nozzle reaction forces can limit the water delivery rate and increase firefighter's fatigue and injuries[3]. Examining which conditions and variables affect nozzle reaction, might encourage investigators to

endeavour new device designs, whom help decrease the jet's kickback in order to facilitate the firemen actions.

In fact, this is a problem which is still on debate in literature, so any contribution to this topic will be invaluable to further progress knowledge and the state-of-the-art.

In conclusion, the results from this research work potentially bear significant impact in the optimization of firefighting mechanisms, in other areas, such as water jet propulsion, and in the creation of knowledge in this field.

1.2. Objectives

The main objective of this research work is the complete waterjet reaction forces characterization and modelling, including the nozzle reaction and hose tension. In the direction of performing a complete data collecting about the mentioned problematic, the strategy applied passed through directly measure the forces exerted in a hose-nozzle assembly, as similar as possible to a real-life situation, possessing recourse to a load sensor.

Simultaneously to the referred data collecting, a theoretical model was developed with the aim of validating and comparing practical results and calculate some unknown variables.

Further objective assumed was to measure the variation of the friction losses due to the hose and nozzle geometry and to compare experimental results *versus* the calculated theoretical values.

1.3. State-of-Art

Water nozzle and hose reactions is still, up to this date, a problem which causes much debate among the scientific community, with few quality works addressing this solution from both a theoretical and experimental point of view.

The most widely disseminated solution is deduced using Newton's third law in a conceptually wrong way, as JW Warren (1975) concluded is very difficult to find conceptually correct explanation for the forces acting on a fire hose[5].

By the above-mentioned reason, a large group of people use the thrust formula for rocket propulsion to calculate this nozzle reaction force, which is not valid because the nozzle is not propelling the water[6]. Is possible to find a few online websites that teach how

to calculate these reactions, although is notable that they blindly use unsourced formulas[7]–[9]. The NFPA book also present some formulas for calculate nozzle reactions[3], unfortunately, no derivation or identification of the assumptions exists, and recent publications have questioned these expressions[6]-[3].

Vera et al. (2014)[6], questioned the existence of this nozzle backward force. In their paper, attempted to prove that a perfectly straight hose will not present this backward force. Vera et al., believed that this backwards force will only appear inside a curved hose, since it is a consequence of the force produced by the water hitting the hose's inner walls. They believed as well that in a straight hose the reaction force is directed forward because the nozzle opposes to the water's flow. They support their idea with a straight elastic hose's experiment, showing that the hose stretches. However, they never address the hose tension to the problem and a perfectly straight hose is not possible in a fire fighting environment.

The first researchers to consider and address this new variable, hose tension, were Chin el al.[3], which, through a seven assumptions problem, reached a formula to calculate this hose tension. However, for this formula to be applied, they assume an inviscid flow and frictionless contact with the ground. This then renders this formula useless in practice. Including this formula in the theoretical model, using the control volume approach to calculate nozzle reaction, only flow's direction forces should appear.

Afterwards, Vera el al. (2018)[10] launched an article that agrees with Chin's et al. paper's calculations but explains why this hose tension formula cannot be used in real life situations. According to Vera et al. (2018), Chin's hose tension formula is difficult to reconcile with a conceptual understanding of the nozzle reaction.

Most of the Fluids Mechanics books[11], neglect the reaction forces of the hose, simply because they are not yet understood. However, they are not always negligible.

In order to analyze and comprehend the reaction forces and torques at the load cell, we followed a Control Volume approach[11].

According to this method, the net change in linear or angular moment inside a Control Volume, equals the net forces and torques acting on the volume. The mentioned forces and torques include those produced by the pressure of water jets cut by the Control Volume, as well as weights of water and other elements enclosed by the volume. Also, the forces and torques of those elements cutted by the surface that delimits the control volume. In our case (further, the used Control Volumes are represented for each case), the surface

that delimits the control volume cuts two elements: the hose and the load cell. The reaction forces and torques at the load cell, which is the point that supports the whole setup, are measured by the mentioned load cell. However, the reaction forces and torques at the hose cannot be easily measured, and they are not easy to model. Thus, since hose forces and moments are the only unknowns in our analysis, we will use all the measured data to solve these forces and moments as the unknowns of our equations. Using the data of the computed hose forces and moments, researchers will be able to model them theoretically in the future, in order to determine how these forces affect the reaction forces measured at the load cell, depending on the geometry of the hose.

This information can be further utilized to minimize reaction forces and torques in the load cell, with the objective that the supporting element (which may be a drone, or the water monitor in a fire-fighting application) is perturbed to a minimum.

2. THEORETICAL MODEL

2.1. Forces and Moments

2.1.1. One Nozzle

2.1.1.1. Forces

With the aim of developing a theoretical model, a control volume is defined containing a hose segment and the nozzle, as seen in figure (2.1):

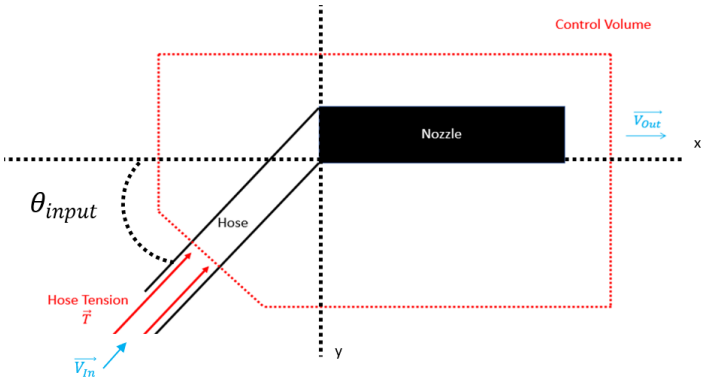

Figure 2.1 - Control Volume adopted

In order to develop the theoretical model, we used the Integral Equation of Linear Movement Quantity Conservation:

$$\sum \vec{F} = \frac{\partial}{\partial t} \iiint_{CV} \rho \vec{V} dv + \iint_{CS} \rho \vec{V} (\overrightarrow{V}.\hat{n}) dA \tag{2.1}$$

Where CV is Control Volume and CS it's surface, ρ the fluid's density, $\vec{V}$ the velocity, $\vec{F}$ represents the forces, $\hat{n}$ the unitary vector and dA the vector pointing out of the control volume. Considering the following assumptions: (1) permanent regime ($\partial/\partial t = 0$); (2) incompressible flow ($\rho = constant$) and (3) uniform velocities for the input and output sections.

Mentioned assumptions transform equation (2.1) in:

$$\sum \vec{F} = \dot{m} \, (\overrightarrow{V_{Out}} - \overrightarrow{V_{In}}) \tag{2.2}$$

Defining, $\dot{m}$ as the mass flow and the *In* and *Out* index refers to the control volume input and output sections.

According to Continuity's Equation is given:

$$\dot{m}_{In} = \dot{m}_{Out} \Leftrightarrow \rho V_{In} A_{In} = \rho V_{Out} A_{Out} \tag{2.3}$$

So, establishing all in terms of the input velocity:

$$\sum \vec{F} = \rho V_{In} A_{In} \left(\frac{V_{In} A_{In}}{A_{Out}} \hat{n}_{Out} - V_{In} \hat{n}_{In} \right) = \rho {V_{In}}^2 A_{In} \left(\frac{A_{In}}{A_{Out}} \hat{n}_{Out} - \hat{n}_{In} \right) \tag{2.4}$$

Now, analyzing the forces exerted on the control volume (the force due to the control volume's weight is neglected):

$$\sum \vec{F} = \vec{R} + \vec{P} + \vec{T} \tag{2.5}$$

The only known force is due to water pressure ($\vec{P} = A_{In} p_{In} \hat{n}_{In}$); $\vec{T}$ appears as the hose tension and $\vec{R}$ is the opposite of the nozzle reaction

Replacing $\vec{P}$ and combining expression (2.5) and expression (2.4):

$$\vec{R} + A_{In} p_{In} \hat{n}_{In} + T \hat{n}_{In} = \rho {V_{In}}^2 A_{In} \left(\frac{A_{In}}{A_{Out}} \hat{n}_{Out} - \hat{n}_{In} \right) \Leftrightarrow$$

$$\Leftrightarrow \vec{R} = \left(\rho {V_{In}}^2 \frac{{A_{In}}^2}{A_{Out}} \right) \hat{n}_{Out} + \left(\rho {V_{In}}^2 A_{In} - T + A_{In} p_{In} \right) \hat{n}_{In} \tag{2.6}$$

In this case, clearly:

$$\hat{n}_{In} \neq \hat{n}_{Out}$$

So, we must distribute the nozzle reaction components according to the referential axes, to predict the R_x and R_y:

$$R_x = (\rho A_{in} V_{in}^2 - T + A_{in} p_{in}) \cos \theta_{input} + \left(\rho \frac{A_{in}^2}{A_{out}} V_{in}^2 \right) \cos \theta_{output}$$

$$R_y = -(\rho A_{in} V_{in}^2 - T + A_{in} p_{in}) \sin \theta_{input} + \left(\rho \frac{A_{in}^2}{A_{out}} V_{in}^2 \right) \sin \theta_{output}$$

2.1.1.2. Moments

In order to develop a theoretical model capable of predict the moments due to the water jet, the same logic and assumptions were established, so we used the Integral Equation of Angular Movement Quantity Conservation:

$$\sum \vec{M} = \frac{\partial}{\partial t} \iiint_{CV} \rho\,(\vec{r} \wedge \vec{V}) dv + \iint_{CS} \rho(\vec{r} \wedge \vec{V})(\overrightarrow{V}.\hat{n}) dA \tag{2.7}$$

With the assumptions previously considered ((1) permanent regime (∂/∂t = 0); (2) incompressible flow ($\rho = constant$) and (3) and uniform velocities for the input section and output section.), the expression (1.7) is given by:

$$\sum \vec{M} = \dot{m}\,(z_{Out}\overrightarrow{V_{Out}} - z_{In}\overrightarrow{V_{In}}) \tag{2.8}$$

Therefore, due to Continuity's Equation (1.3):

$$\sum \vec{M} = \rho V_{In} A_{In}\,(V_{Out} z_{Out} \hat{n}_{Out} - V_{In}\, z_{In} \hat{n}_{In}) \tag{2.9}$$

This theoretical approach assumes a two-dimensional problem (forces only exist on the plane XY), so the only resulting moment is around the z axis:

$$\sum \vec{M} = M_z - P z_{In} \hat{n}_{In} + \mathrm{T} z_{In} \hat{n}_{In} \tag{2.10}$$

Combining equation (1.9) and equation (1.10), and given that $\vec{P} = p_{In} A_{In}$:

$$M_z = (\rho V_{In}^2 \frac{A_{In}^2}{A_{Out}} z_{Out}) \hat{n}_{Out} - (\rho V^2{}_{In} A_{In}\, z_{In} - p_{In} A_{In} z_{In} + T z_{In}) \hat{n}_{In} \tag{2.11}$$

2.1.2. Two Nozzles

In order to develop a theoretical model for the nozzle with two outputs, a control volume was defined (figure 2.2):

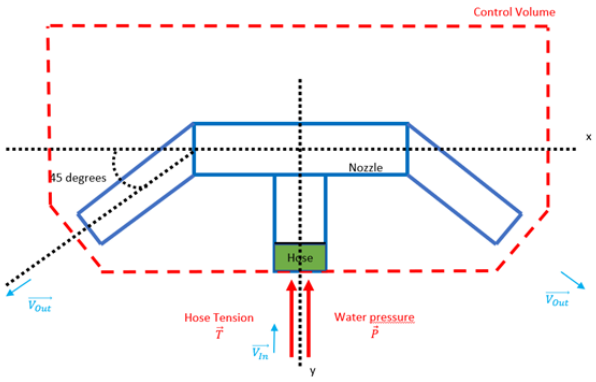

Figure 2.2 - Control Volume adopted for Two-Outputs' theoretical model

As can be observed in the above-displayed control volume, since the nozzle is symmetric along the y axis, the two output velocity's components along x axis will cancel (assuming $\dot{m}_{In} = 2\dot{m}_{Out}$), therefore, exclusively an analysis along the y axis is necessary (in the theoretical model, no forces along the x axis should appear).

Employing the same assumptions as the previous theoretical model, the Integral Equation of Linear Movement Quantity Conservation, can be expressed as:

$$\sum \vec{F} = \dot{m}\,(\overrightarrow{V_{Out}} - \overrightarrow{V_{In}}) \tag{2.12}$$

Performing an analysis along the y axis, that in this case, coincides with vector $\hat{n}_{In}$:

$$\sum F_y = \dot{m}\,(2V_{Out}\cos(\theta) - V_{In})\hat{n}_{In} \tag{2.13}$$

Now observing the exerted forces:

$$\sum F_y = \vec{R} + \vec{P} + \vec{T} \tag{2.14}$$

Equalizing equation (2.13) and (2.14), knowing that $\vec{P} = A_{In}p_{In}\hat{n}_{In}$ and $\theta = 45^o$ [figure 2.2], and assuming $\dot{m}_{In} = 2\dot{m}_{Out}$:

$$R_y = (-T - A_{In}p_{In} + \frac{A_{in}^2}{A_{out}}V_{in}^2\cos 45° - \rho {V_{In}}^2 A_{In})\hat{n}_{In} \tag{2.15}$$

From the theoretical model for the two inclined outputs, it is simple to understand that for the vertical outputs, the difference will be that we must not distribute the output velocity's components along the x axis, practically, the only difference between them is the absence of term $\cos 45°$ in equation (2.15), so for the two vertical outputs' case the referred equation must be written:

$$R_y = (-T + A_{In}p_{In} + \frac{A_{in}^2}{A_{out}}V_{in}^2 - \rho {V_{In}}^2 A_{In})\hat{n}_{In} \tag{2.16}$$

In this case, no moments should be associated, considering that all the forces exerted on the control volume are applied in the origin and a two-dimensional problem was assumed.

2.2. Friction Losses

A pump obeys to the following equation, that can be derived from the generalized Bernoulli's equation including a pump:

$$(\frac{p}{\rho g} + \frac{V^2}{2g} + z)_{output} = (\frac{p}{\rho g} + \frac{V^2}{2g} + z)_{input} + H \tag{2.17}$$

Where p is the pressure, V the velocity, ρ the fluid's density, z the height, g represents the gravity's acceleration, H is the "energy" that the pump adds to the fluid, but it is measured in units of length.

As we are using relative pressures, as the flow is developed in atmospheric conditions the output pressure is equals to zero. Assuming the water height remains nearly steady in the pump's tank and no difference between input and output heights, equation (2.12) can be written as:

$$(\frac{p}{\rho g} + \frac{V^2}{2g})_{output} = H \tag{2.18}$$

Considering the pump's output (hose + nozzle) the load circuit that the pump must overcome. The water's energy loss H within the hydraulic circuit can be written as [11]:

$$H = kV^2 \tag{2.19}$$

Where V is the velocity and "k" is a constant that depends on the losses of fluid pressure along the hydraulic circuit that depends on the roughness of the internal surface of

the hose, on the Reynolds number, on the length of the hose, and on the presence of abrupt changes of section. Combining both equations (2.13) and e (2.14):

$$(\frac{p}{\rho g} + \frac{V^2}{2g})_{Output} = kV^2 \tag{2.20}$$

Also, is given that the velocity can be calculated dividing the flow (q) for the cross-section's area of the hose ($q = VA$), so placing all in order to solve the flow in terms of pressure:

$$q = A\sqrt{\frac{p}{\rho(kg - \frac{1}{2})}} \tag{2.21}$$

This "k" value sums all losses due to friction and obstacles that the fluid finds within the circuit and it is often difficult to estimate analytically.

3. EXPERIMENTAL STAGE

The present chapter contains a complete and detailed description of the performed experiments. The first task of this experimental stage was to calibrate our measuring device, the JR3 load sensor, model 67M25. After this, four more experiments were made:

- Horizontal nozzle experiments
- Input and output angle variation
- Two-output nozzle experiments
- Friction loss experiments

3.1. Load Sensor Calibration

In order to correctly interpret the data collected by the load sensor, a sensor calibration had to be performed, so that one could relate the sensor digital signal output to an actual force or moment. The mentioned calibration's final objective was to attain the 6 linear equations (three axis and three moments) that transform sensor response (digital signal) into actual quantities of force and moment. Basically, the purpose was a description of the load sensor behaviour while exerting known forces, to acquire a data base that allow us to understand the signals returned by the sensor while responding to unknown forces.

3.1.1. Material

Toward execute the load sensor calibration, the follow materials, displayed in figure 3.1, were required:

a) JR3 load sensor and its respective software

b) Iron weights (1, 2 and 5 kg)

c) Steel wire to secure the iron weights

d) Support disc to be attached to sensor with superior diameter

e) Weight support rod

f) Structure that support all the experimental components

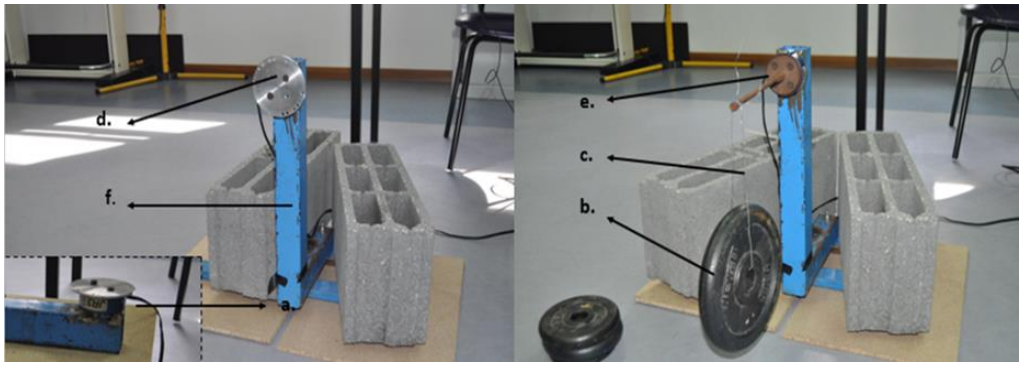

Figure 3.1 - Calibration Trial required material

3.1.2. Load Sensor Characteristics

The multi-axis load cell by JR3, also regularly known as a 6 degree-of-freedom force-torque sensor, is a cylindrical aluminium device containing analog and digital electronic systems. Foil strain gages connected to multiple internal load-bearings sense the loads imposed on the cell. The strain gage signals are amplified and combined to produce analog representations of the forces along three orthogonal axes (x, y and z) besides the moments around those axes. In the end, the electronic systems within the load cell convert these analog signals into digital. The x and y axes are oriented at the horizontal midplane of the sensor body and z axis is coincident with the normal vector of this plane, positioned in the sensor's centre. The reference point for all the measurements it's the sensor's geometric centre. In this test was used the 67M25 I40 model, with digital output. The 2D draw of the sensor is placed in Annex A, figure 0.1.

3.1.3. Procedure

3.1.3.1. Calibration trial for z axis force

In order to perform the test, the structure was positioned horizontally, so the z axis was oriented along the vertical direction. The lead discs, with known weight, were placed gradually on the load cell. Simultaneously, the values exhibited by the sensor's software were saved in an Excel document. As demonstrated by figure 3.2, the cell was loaded with 1, 2, 3 ,4 and 5 kg weight masses.

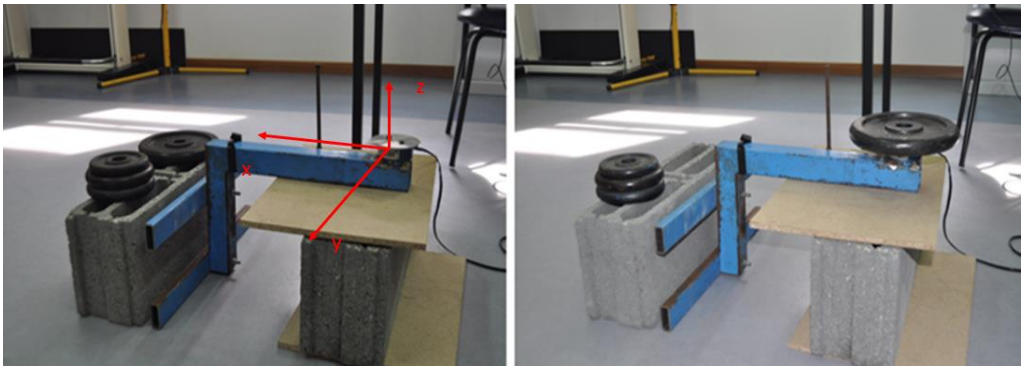

Figure 3.2 - Calibration trial assembly for z axis force

3.1.3.2. Calibration trial for z axis moment

The structure was placed in its original position (vertically). As depicted in figure 3.3, an aluminium disc, with diameter superior to the load cell, was anchored concentrically to it. Toward create a known distance between the point where the force was applied and the sensor's centre. The mentioned distance was measured employing a simple digital calliper. Similarly to the previous test, the iron weights were placed gradually and the presented values (for 0, 1, 2, 3, 4 and 5 kg) were saved. The iron weights were hung, applying the wire, at the border of the aluminium disc ensuring no interference with the surrounding objects.

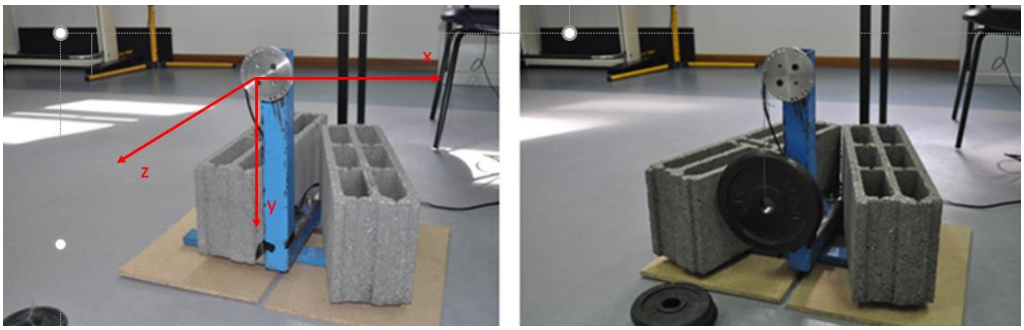

Figure 3.3 - Calibration trial assembly for z axis moment

3.1.3.3. Calibration trial for x axis moment and y axis force

Towards perform this test, a small rod, with known length (measured employing the digital calliper), was attached perpendicularly to the sensor face. Obtained this known length, between the point where the force was exerted and the sensor centre, enabled us to evaluate the x axis moment, besides the y axis reaction force. The weights were now hung, applying the wire, in the beam's extremity and the previous tests' method was applied, as demonstrated in figure 3.4, in order to record the data.

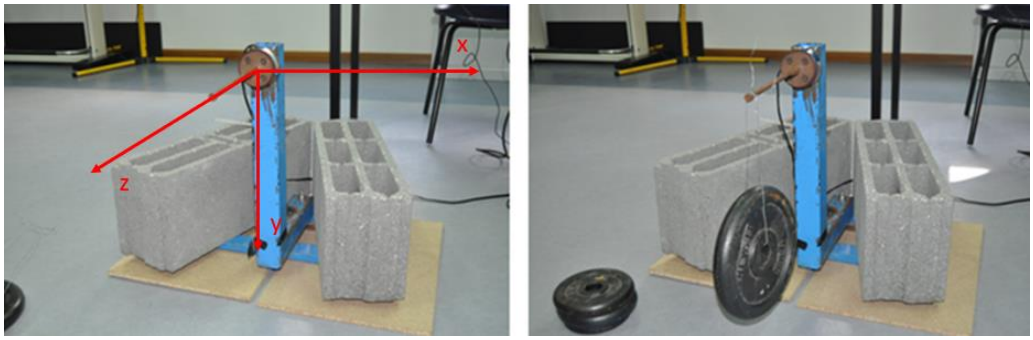

Figure 3.4 - Calibration trial assembly for x axis moment and y axis force

3.1.3.4. Calibration trial for x axis moment and y axis force

The above-mentioned test proceeded exactly as the previous one, except the fact that the load sensor was rotated 90 degrees, so the x axis orientation would be along the vertical direction.

3.1.4. Results and Data Processing

Knowing the corresponding sensor signal to each force and moment produced in the previous experiments, with the weights of 1 to 5 kg, one could produce the graphs for Force or Moment as a function of the load cell digital output. (figure 3.5). Finally, through the least squares' technic, one was able to obtain the equation of the line that better describes the sensor's response, for each axis.

In our case, we are solely interested in the line gradient, since the line always intersects the referential origin. Notice that the graphics that describe x and y axes moments uniquely display loads until 3 kg, because larger weights caused the sensor to saturate.

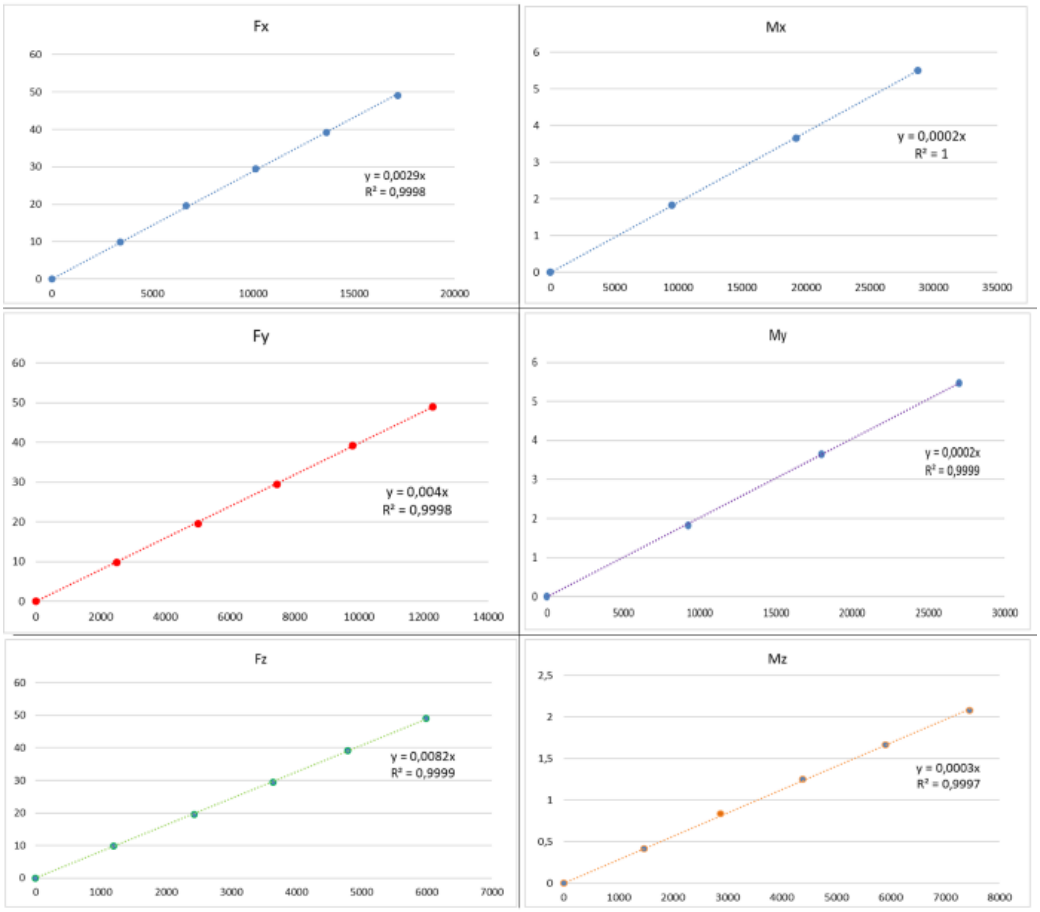

Figure 3.5 - Calibration graphics (Force (N)/Moment (N.m) vs Sensor signal)

Luckily, the load cell had an extremely linear behaviour, which, besides facilitating this calibration, conceded us the ability to extrapolate these results for any unknown load. Table 3.1 displays the calibration line gradients which allow us to convert the sensor's digital output signals in corresponding forces and moments. (note: the complete RAW data extracted is display in Table 0.1, annex A.

Table 3.1 - Calibration Lines Gradient

Reaction / Moment	Calibration Line Gradient
F_x	$2{,}9 \times 10^{-3}$
F_y	$4{,}0 \times 10^{-3}$
F_z	$8{,}2 \times 10^{-3}$
M_x	$2{,}0 \times 10^{-4}$
M_y	$2{,}0 \times 10^{-4}$
M_z	$3{,}0 \times 10^{-4}$

3.2. Horizontal nozzle experiments

The horizontal nozzle experiments' subchapter contains a detailed description of the first experimental test performed with the aim of execute a complete modelling of the forces exerted in a water ejecting nozzle. The mentioned description begins with the list of required material, then the methods and procedures used, followed by the experiment results presentation and its interpretation.

3.2.1. Materials

For the nozzle first test the follow materials, displayed in figure 3.6 were required:

a. 1" Commercial Nozzle
b. JR3's load sensor
c. Support structure
d. Computer for data acquisition
e. Aluminium support part to fix the nozzle in the sensor
f. Hydraulic pump
g. 1" Commercial hose
h. Analog pressure gauge

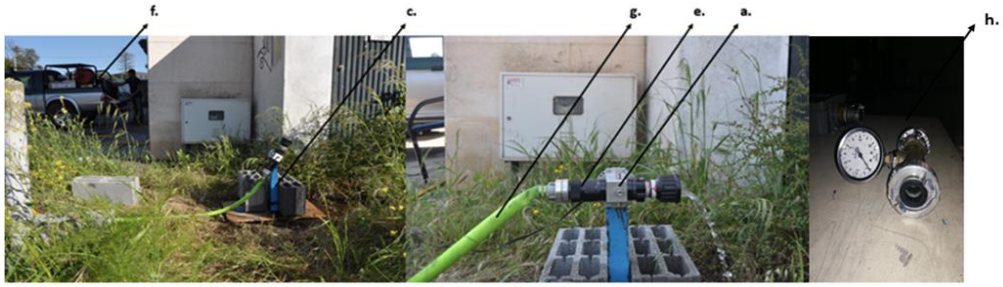

Figure 3.6 - Horizontal angle experimental setup

3.2.2. Procedure

The method performed for the Horizontal Angle Experiment, basically, consisted into coupling the commercial nozzle on the load sensor, applying the aluminium support part. The mentioned aluminium support part was composed by a disc, placed

stationary and concentrically on the sensor, and a metal clamp that anchored the nozzle and was screwed on the aluminium disc, as depicted in figure 3.7. This same disk allowed to variate the nozzle angle between three positions: 0º, 30º and 60º.

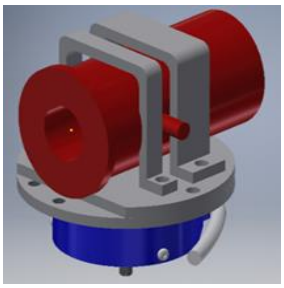

Figure 3.7 - Nozzle and sensor assembly scheme

Afterwards the pump was switched on, connected to the nozzle, through the commercial hose.

At that point, the pump service pressure was increased slowly from 0 to 10 bar, and the load cell digital output signal was manually recorded in an Excel document, for the pressures of 1, 2, 3,.. up until 10 bar.

This test was repeated for four initial conditions, that can be seen in figure 3.8. Discriminating: (A) 30-degrees nozzle; (B) 60-degrees nozzle; (C) 0-degrees nozzle with no hose support and (D) 0-degrees nozzle, hose supported. To summarize, the forces and moments were measured with the nozzle describing 0, 30 and 60-degrees angle relative to the horizontal plane, and with no hose support. For 0 degrees, another test was executed with the hose maintained straight and horizontal before the nozzle.

Figure 3.8 - - Horizontal Angle Trial initial conditions

3.2.3. **Results and Data Analysis**

Table 0.2, available in annex A, displays the results after being processed, so, the digital signals are already transformed into the corresponding force or moment. In order to present the results to the reader, the followed graphics were designed [figure 3.10] (for better comprehension of the results, observe figure 3.9):

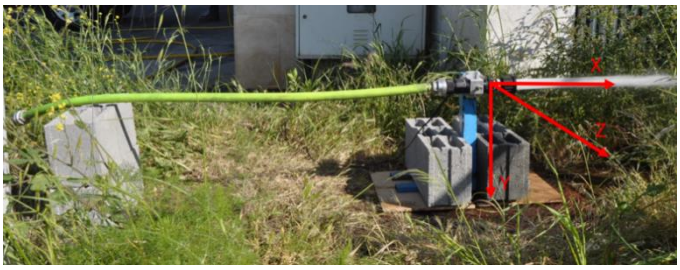

Figure 3.9 – Experiment's axes display

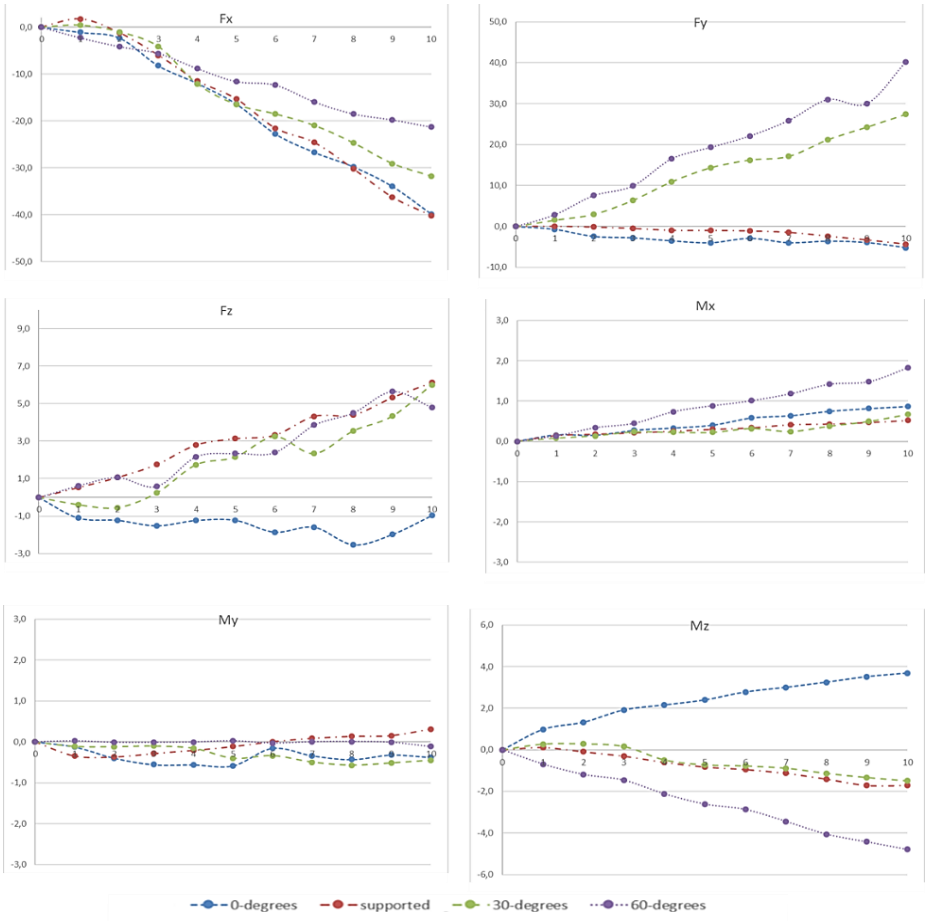

Figure 3.10 - Horizontal nozzle experiment results (Force(N)/Moment(N.m) vs pressure (bar))

This first nozzle's test gave us the opportunity to reach some conclusions. The main observation target of our experiment were the reactions along the x and y axes and the moment around the z axis, since were the reactions expected to be the highest. The previous sentence can be proven observing the results that present residuals values for these three degrees-of-freedom.

As expected, in the horizontal nozzle's tests the kickback or reaction force had its bigger component within the x axis (the positive x axis' direction points to the waterjet flow, that's why the values are negative). When we increase the nozzle's angle (to 30 and 60 degrees) we start to distribute the kickback force components between the x and y axes. Practically, means a decrease in the x axis' component and an increase in the y axis' component.

For the "30 degrees" and "0 degrees supported" assemblies the z axis momentums are considerably lower than for the other two assemblies, which reveal that linear hose-nozzle systems, lower the z axis momentum. As we can see by the test photos, the "60 degrees" and "0 degrees without support" created an elbow in the hose right before the nozzle figure 3.11. Analysing the magnitude and direction of the created momentum is possible to notice that the tendency of system, due to the flow inertial forces, is to undo the elbow figure 3.11. The considerable difference in the momentum magnitude between the two assemblies mentioned can be explained by the ground constraining. In "0 degrees without support" assembly the hose can move in the direction of the inertial forces solicitations, with the increasing of pumper's service pressure the hose-nozzle system became more linear, decreasing the elbow's magnitude. In "60 degrees" assembly case, when the hose tries to move in the direction of the inertial forces solicitation it finds the constraining of the ground, which keeps the elbow in the same position during the whole test, that explains the higher z axis momentum. In figure 3.11 we can see this hose's movement in the "0 degrees without support" assembly comparing the hose position between the "pump off" picture and the "pump on" picture, besides the z axis momentums direction. Also, comparing the two "60 degrees" assemblies' pictures is possible to see that the hose practically did not move.

Figure 3.11 - Pump on vs pump off; On top: 60-degrees assembly; on bottom: 0-degrees

Table 0.4, available in annex A, exhibit the resultant's kickback force value for each assembly and for each service pressure tested, calculated by the magnitude of the three reaction components.

Theoretically, the resultant force should be the same within every assembly tested, for each service pressure. The nozzle reaction doesn't depend on the jet angle. This doesn't verify in our results but can have various explanations. Within these explanations is the deformation of the metal clamp that fixes the nozzle in the sensor, caused by the kickback force itself. Another one is the imprecision of the pressure reader device. We used an analog manometer with pointer technology, that doesn't guarantee that the sensor's signals were saved in the right pressure (for example the signal returned by the sensor for the 1 bar pressure, can be saved when the pumper's service pressure was at 0.9 bar or at 1.1 bar).

This first test, basically, showed us the importance of studying the effect of the hose bend in the nozzle reaction.

3.3. Input and output angle variation

The focus of the second set of experiments, was, the effect of the variation in the water input and output angles, in the nozzle reaction variation. The crucial difference between this test and the previous is the analysed variable. The central variable investigated changed from the angle created between the hose and the horizontal direction to the two input and output angles.

3.3.1. Material

The material employed in this test was identical to the previous, except for the aluminium part responsible to fix the nozzle on the sensor face that was replaced. A new aluminium support part was designed to allow the variation of the angles of the setup. This new support part allows to control the input flow angle (hose angle) continuously from 0º to 90º, and the output flow angle (nozzle angle) between three positions: 0º, 45º and 90º [figure 3.12].

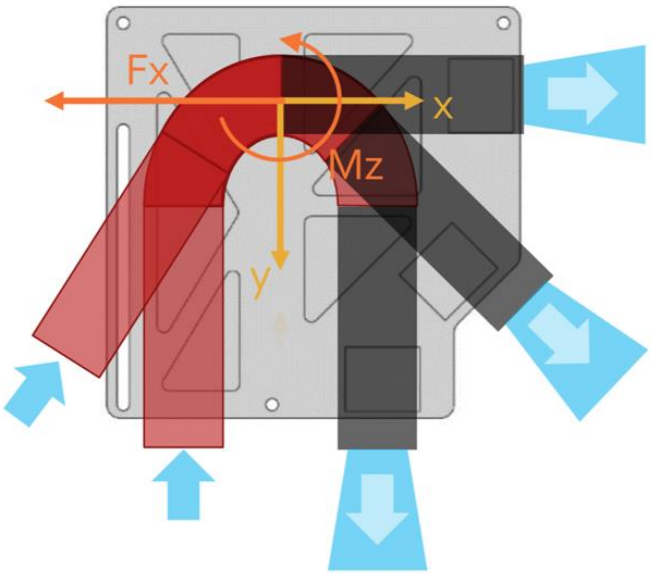

Figure 3.12 - New device responsible to fix the nozzle

3.3.2. Procedure

Procedures within tests are similar, since the essential idea remains the same. The variables were now the input flow angle and the output nozzle angle. Test was repeated for 4 input different angles and 3 output angles, which is a total of 12 trials. Data collecting method was repeated. For each input-output angle combination, pump service pressure was increased from 0 bar to 10 bar and the returned signals from the sensor were saved for every pressure integer value.

3.3.3. **Results**

Complete experiment results can be seen in the Annex A, Table 0.5. It follows, in figures 3.13, 3.14 and 3.15, the graphics that describe the magnitude of the reaction values:

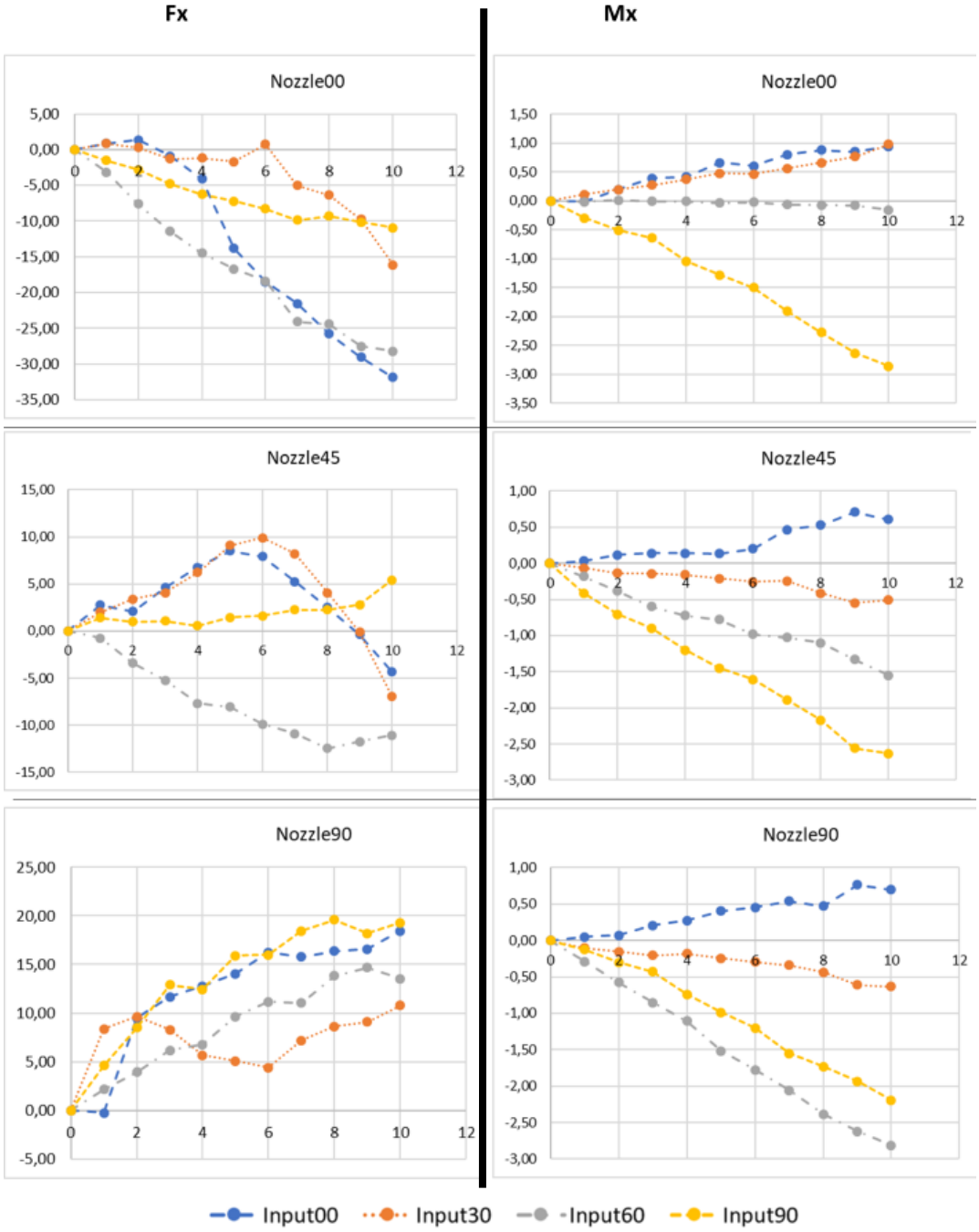

Figure 3.13 - Graphics whom display the x axis results(Force(N)/Moment(N.m) vs pressure (bar))

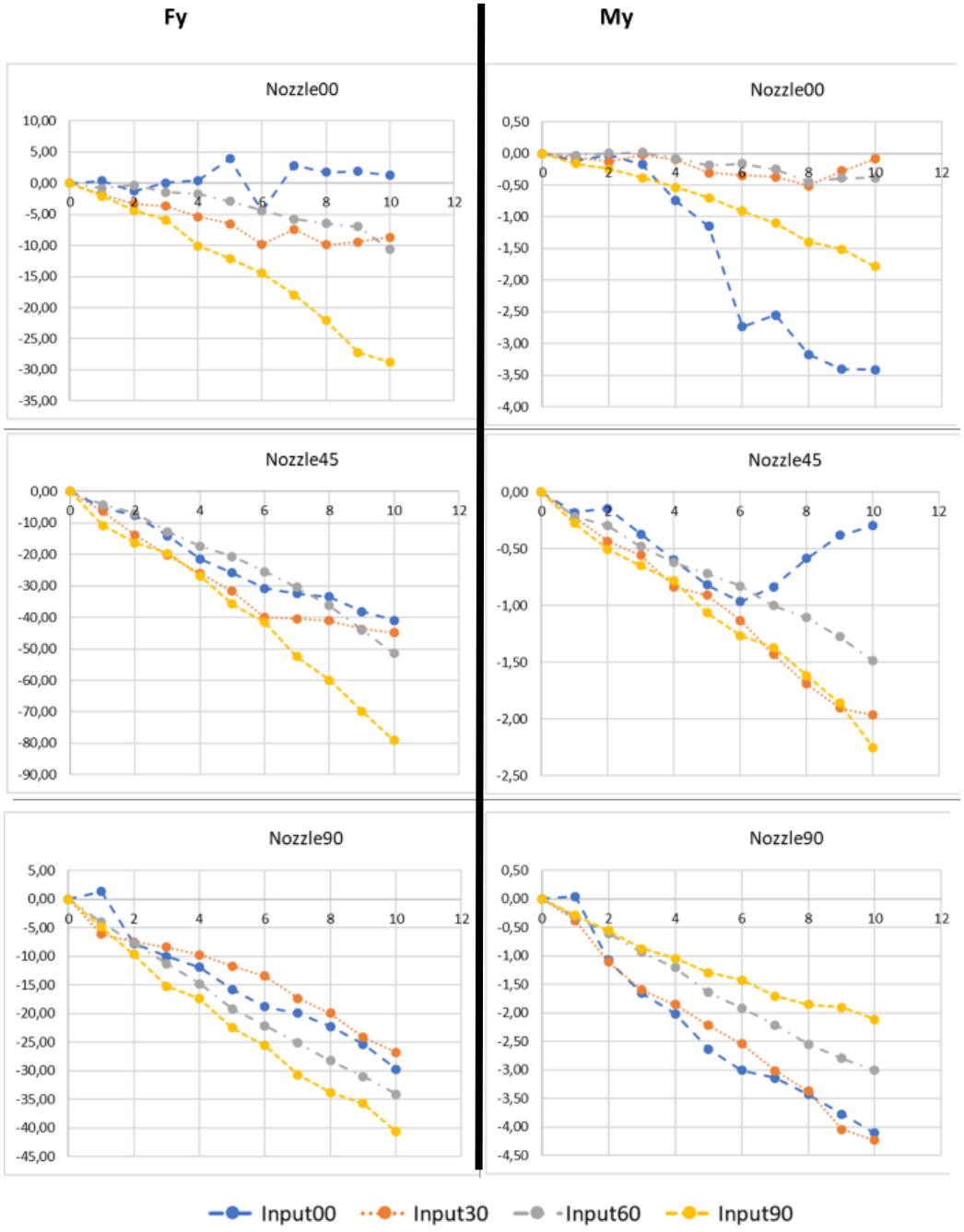

Figure 3.14 - Graphics whom display the y axis results(Force(N)/Moment(N.m) vs pressure (bar))

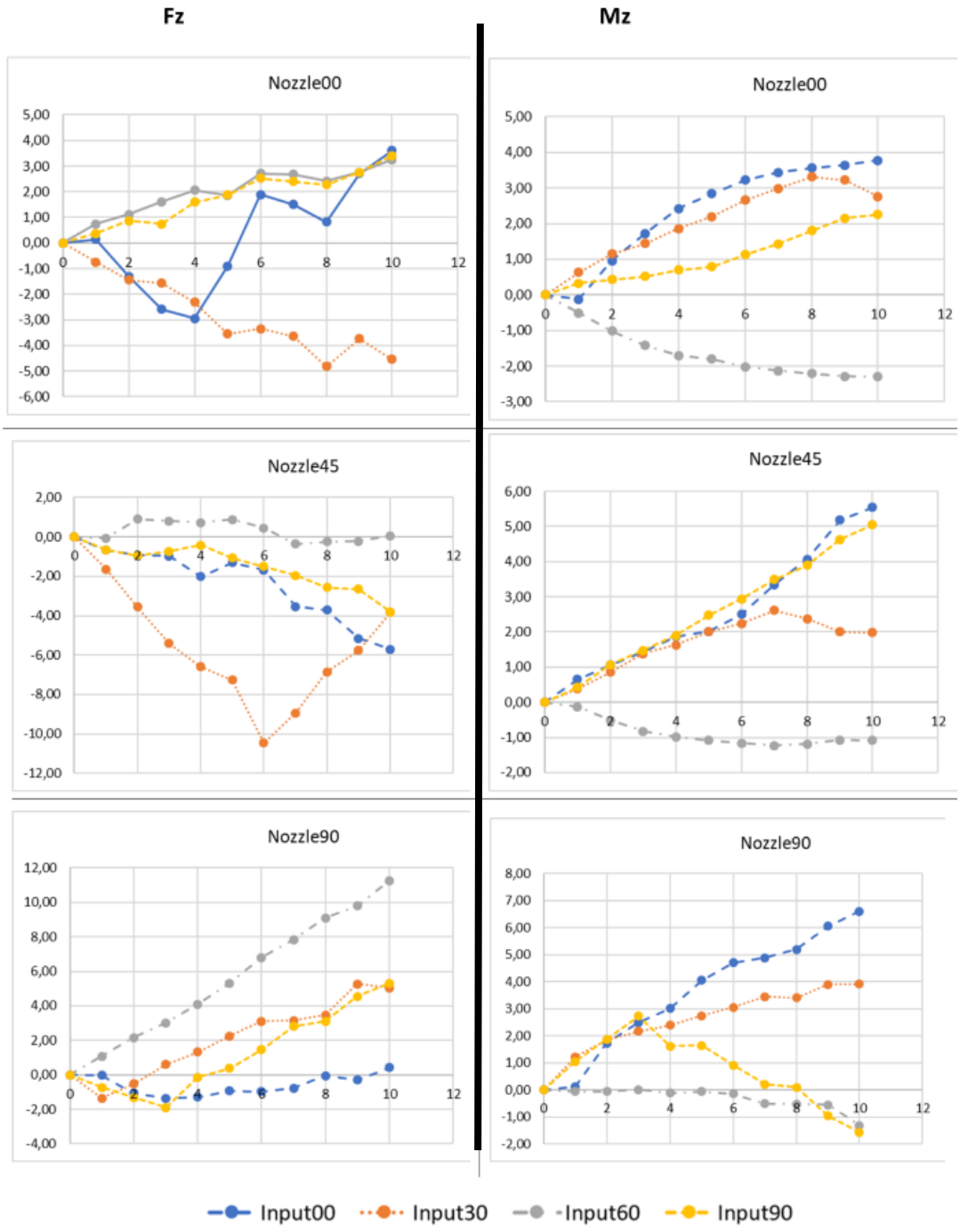

Figure 3.15 - Graphics whom display the y axis results(Force(N)/Moment(N.m) vs pressure (bar))

As depicted in the reaction's graphics, and as expected, the higher reaction attained along the x axis, was obtained for the most linear hose-nozzle geometry's assembled (0 degrees input angle; 0 degrees output angle) [figure 3.16].

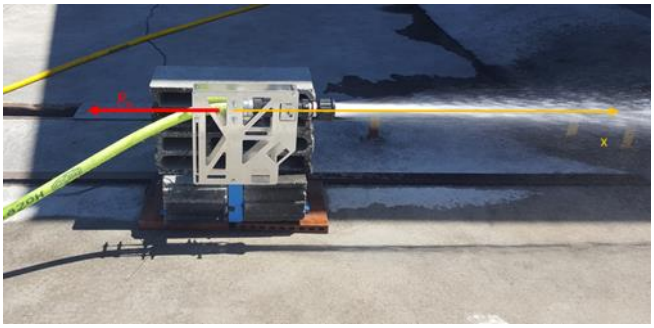

Figure 3.16 - Linear geometry's reaction direction

Is interesting to notice as well, that when the nozzle is placed on the 90-degrees position [figure 3.17], the exerted force on load cell changed its direction. Was assumed that it was a result of the "propulsion" force was directed vertically, so the largest component along the horizontal direction, was due to hose tension and water pressure. Considering that the higher value obtained was near 19 N. Assuming 1" hose, and the maximum pump's service pressure (and it's lower due to friction losses), the higher force due to water pressure should be, theoretically, around 0,5 N. Hose tension should be responsible for this values difference. Once again, it proves that hose tension should not be neglected.

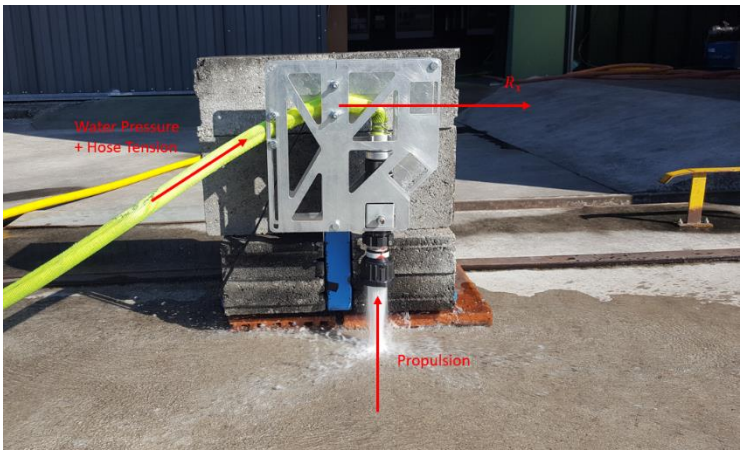

Figure 3.17 - 30degrees input-90degrees output reaction force direction

The 90-degrees hose's position combined with the 90-degrees nozzle's position, should present residuals reactions along x axis, instead it presents the higher value. It could be explained by the following observation: in the zone spotted with a red circle in figure 3.18, is notable a hose's section constriction, due to the U-bend, the mentioned constriction opposes the water flow, what could create a reaction force in that zone directed along the flow direction. Vera et al. (2014) demonstrated that this reaction exists[6].

Figure 3.18 - 90 degrees input and output assembly

Hose's tension force exertion endeavour overcome friction losses (due to hose bends) and place the hose as linear as possible, so is reasonable that similar input and output angles geometries decreases the moment around the z axis. By reason that similar input and output angles create an almost symmetric hose-nozzle position, referred to the y axis. So, the hose moment around the z axis should cancel the nozzle moment [figure 3.19].

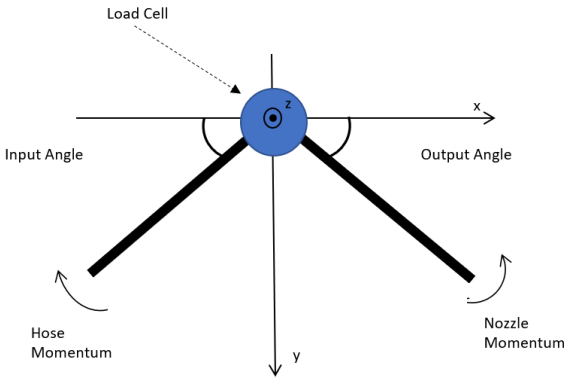

Figure 3.19 - Balanced moment scheme

To finish this subchapter is important to notice that theoretically the force along the z axis should not exist if the hose was disposed in the XY plane of the setup. However, as can be seen in figure 3.20, the hose was not perfectly directed along the XY plane, so the forces due to hose tension and water pressure created a reaction component along the z axis too.

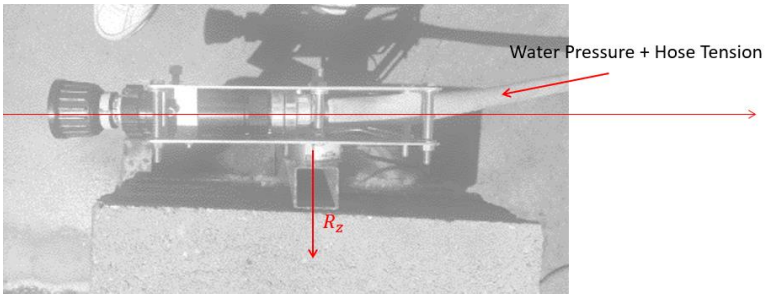

Figure 3.20 – Experiment's top view

3.4. Two-outputs nozzle experiment

Two-outputs nozzle experiment main goal was towards trying to eliminate all forces and moments along the horizontal plan, also was tried to obtain the force along the vertical plan, reducing as much as possible the moments within the referred plan. The mentioned setup is an approach to drone application and the purpose is to identify the better nozzle's geometry to be attached to the drone.

3.4.1. Material

To perform the mentioned test, two new setups containing two symmetric nozzles each, were made. The first setup has the two outputs pointing directly to the ground (perpendicularly to the horizontal direction) (90-degrees nozzle; figure 3.21),

Figure 3.21 - 90-degrees nozzle

The other setup outputs create a 45-degree angle relative to the horizontal direction (45-degrees nozzle; figure 3.22).

Figure 3.22 - 45-degrees nozzle

Because of the different nozzle's design, a new support to fix the nozzle to the sensor was designed as well, as seen in figure 3.23.

Figure 3.23 - New device responsible for fixing the nozzle

3.4.2. **Procedure**

As aforementioned, the procedure is similar within performed tests (increasing pressure and register the reactions). This time, due to the limitations of the pump flow used, it was not possible to go beyond 5 bar of pressure since the water flow, due to the use of two output nozzles, duplicated in relation to the previous single output tests.

Three experiments were performed. Two for the 90º nozzle, with different hose arrangement (vertical and inclined), and one for the 45º nozzle. For each experiment, five trials were made.

3.4.3. **Results**

As above-mentioned, five trials were implemented for each initial condition, thus, figure 3.24 displays the graphics containing the average among the reactions measured between them. Complete average results can be seen in Table 0.6, available in annex A.

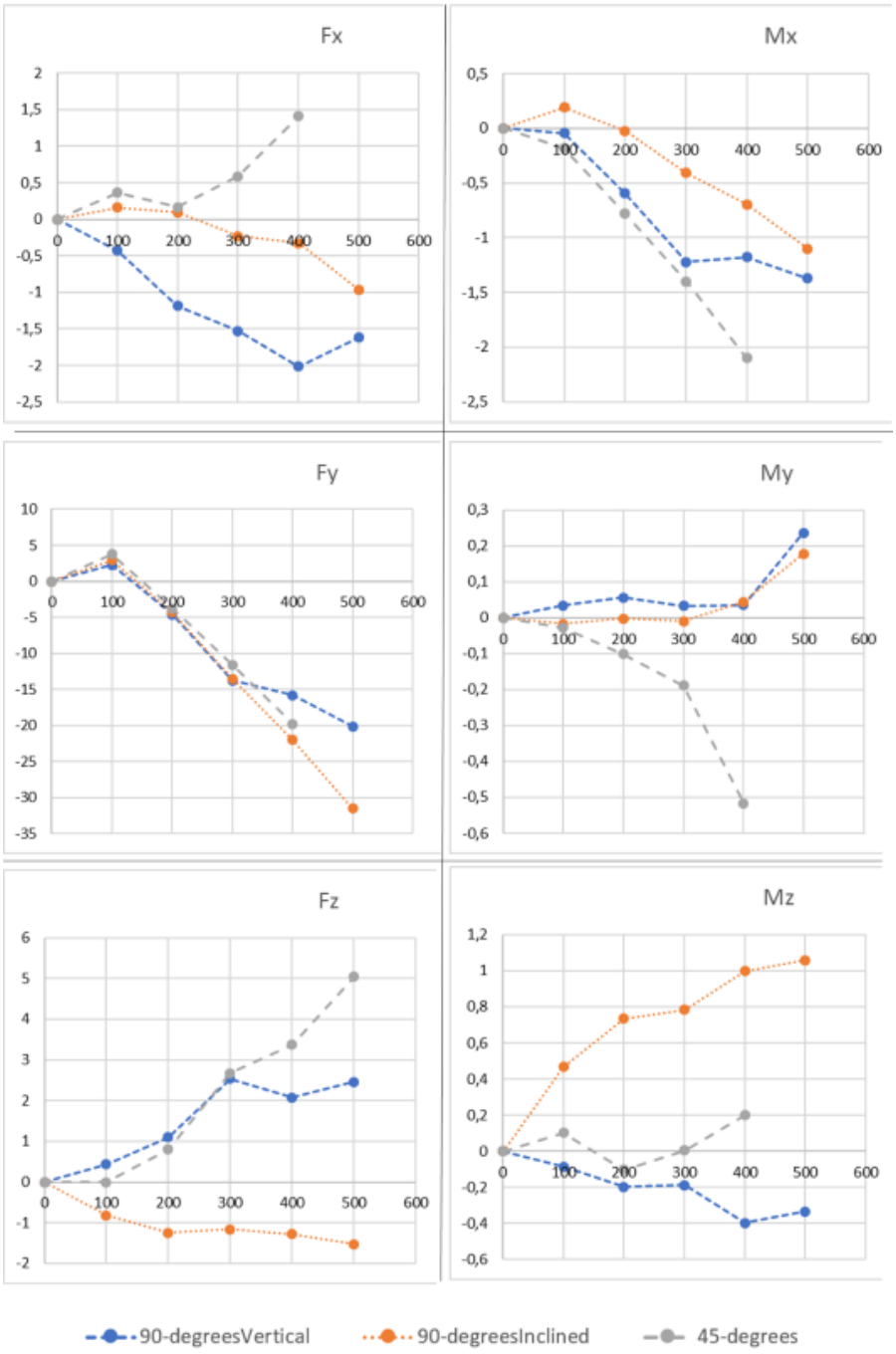

Figure 3.24 - Graphics whom display the two-output's trial results

As expected, the reactions along the horizontal axis were residual. As explained in the theoretical model developed in subchapter relative to the two-outputs force, 90-degrees nozzle's case contains no forces along the horizontal direction and the x axis reaction components present by the 45-degrees nozzle's case, cancels each other.

As can be seen in figure 3.24, the moments around the y axis could be neglected, by reason that the extracted values are way lower than the other moments.

The most interesting conclusion to obtain, observing these results, is that the hose position is the key to comprehend nozzle reactions. The previous conclusion is supported by two main reasons: 1) hose vertical input implies higher moments around the x axis; the force along the z axis was positive while the vertical input was implemented, and negative while the inclined input was implemented; 2) the force along the y axis increased around 50% while the inclined input was implemented.

Now I will explain, one-by-one, the previous reasons:

1) As above-mentioned, the hose tension endeavour overcome the pressure losses, practically, the hose tension result is forces trying to place the hose as linear as possible. In the figure 3.25, is possible to see the moments created (the red curved arrows) by the hose inner forces, in order to place the hose as linear as possible. The right-side moment, in figure 3.25, is supported by the ground, the left one is responsible for the high moments around the x axis. The moment previous mentioned is responsible for a positive force along the z axis. While in the inclined input assembly, negative z axis forces were registered.

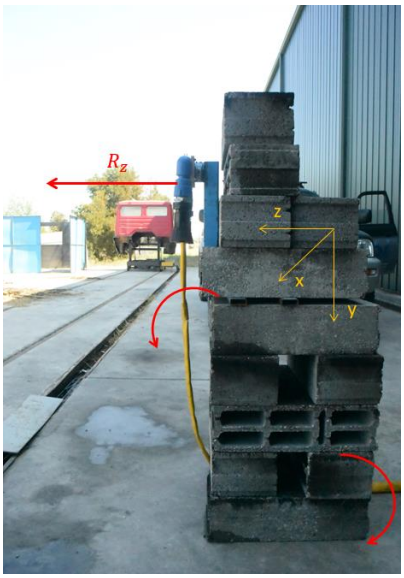

Figure 3.25 - 90-degrees vertical input trial

2) The reason for the force along the y axis increased almost 50% while the inclined-input was implemented, is due to the hose inner forces trying to place it linear, again. The hose segment placed between the load cell and the rock (figure), since is “locked” in the referred two points, the only way it has

to become linear is creating the moments presented in figure, represented by the red curved arrows. Whose will result in a force directed like figure displays employing a linear red arrow. Part of this force will, clearly, be supported by the load cell, increasing its reaction (figure 3.26 displays the pump off situation, in order to better comprehend the above-mentioned effect, a pump on situation's scheme was elaborated [figure 3.27]). Another evidence of the referred force is the higher moment around the z axis, when compared to experiments implementing the vertical input.

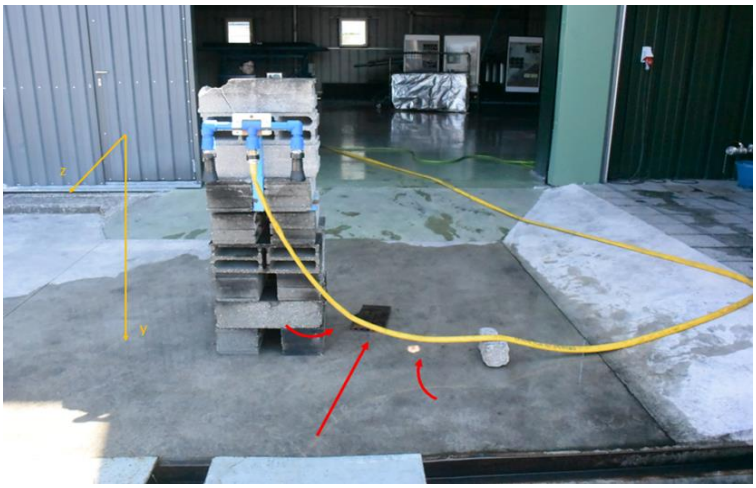

Figure 3.26 - 90-degrees inclined input trial

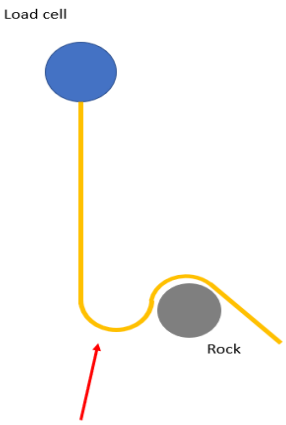

Figure 3.27 - Inclined input trial (pump on) scheme

3.5. Friction loss experiment

In order to calculate the input velocity in the control volume, a friction loss estimation within the load circuit (nozzle and hose) was essential, hence an experimental test was designed with the aim of estimate the mentioned friction losses in the hose and nozzle setup and varying the hose angle.

3.5.1. Material

Exclusively an additional flowmeter was applied to control the pump output flow, displayed in figure 3.28, on the left. It was assembled as shown by figure 3.29, on the right.

Figure 3.28 - Flowmeter and its assembly

3.5.2. Procedure

Was considered that pump's output flow data collecting wouldn't be affected by the hose-nozzle system's input and output angle. Just in case, the test was performed assembling two different hose positions [figure 3.39] (using the input and output angle variation trial assembly) towards compare the results within positions (5 tests for each position). Trial's procedure consisted in connecting the flowmeter between the pump and the hose and save the displayed flow amount for each pressure value between 0 and 10 bar.

Figure 3.29 - The two assemblies tested within this trial

This experiment was performed as well for the two-outputs nozzle case, however it does not fit as well in the theoretical model, since it was developed for the one-output nozzle only.

3.5.3. Results

3.5.3.1. One output

The referred test required a data processing operation, exploiting the theoretical model displayed in subchapter 2.2.

Pump's output flow results are in Table 0.7, where it can be seen the flow's values measured and its average, for each input angle and pump's pressure tested. The referred table presents the "K" value that optimized the results and the theoretical flow values calculated by equation (2.16). Instead of finding this value with a theoretical method, we did it by trial-and-error, varying the "k" value until the theoretical values matched the experimental data.

Value which represents better our hose friction losses due to its roughness, diameter, path bends and length:

$$K = kg = 210$$

Assuming a 1-inch hose's diameter and $g = 10\ m/s^2$.

Afterwards, the 1-output control volume's input velocity was calculated from the pump's output flow theoretical values.

Table 3.2 presents the control volume's input velocity in terms of pressure. Friction Losses test conceded us the necessary data to conclude that the velocity only depends on the service pressure, the hose's input angle does not affect it.

Table 3.2 - Control Volume's input velocity for each pressure

Pump's Service Pressure [bar]	Control Volume's Input Velocity [m/s]
1	0,69
2	0,98
3	1,20
4	1,38
5	1,54
6	1,69
7	1,83
8	1,95
9	2,07
10	2,18

3.5.3.2. Two outputs

Since these results do not fit in theorical model developed for one-output, this subchapter will only display the results obtained employing the flowmeter attached to the pump output, in figure 3.30:

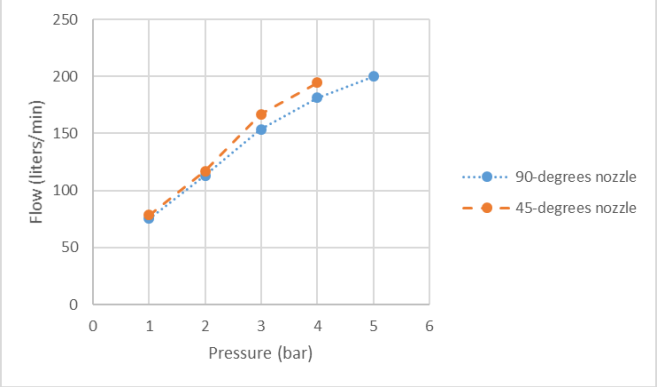

Figure 3.30 - 90-degrees vs 45-degrees nozzles flow

As expected, the two-outputs nozzle possess roughly twice the water flow of a single nozzle. One can also observe a higher water flow for the 45-degree nozzle when compared with the 90-degree setup. This can be attributed to lesser hydraulic losses for the 45-degree bend in the nozzle, when compared with the 90-degree bend.

4. THEORETICAL MODEL VS EXPERIMENTAL RESULTS

4.1. Chin's theoretical model

Chin et al. (2017), as above-mentioned, developed a theoretical model which objective was to reach an expression towards calculate the hose tension force. Through a seven-assumptions problem the followed formula was achieved:

$$T = p_{in}A_{in} + \frac{\rho q^2}{A_{in}} \tag{4.1}$$

Replacing T in this report's theoretical model will result in Chin et al. (2017) expression to estimate nozzle reactions as well:

$$\vec{R} = \frac{\rho v_1^2 A_1^2}{A_2}\hat{n}_{Out} \tag{4.2}$$

This contradicts all the experiment's results achieved, since it implies that reaction forces only appear on the jet output direction (for example, for the input and output angle variation experiment with nozzle on the 0-degrees position, only x axis reaction forces should appear). Examining figure 4.1 is simple to comprehend that the previous expression cannot be used in practical situations, since the forces obtained along the y axis for some configurations are as high as the forces obtained for the x axis.

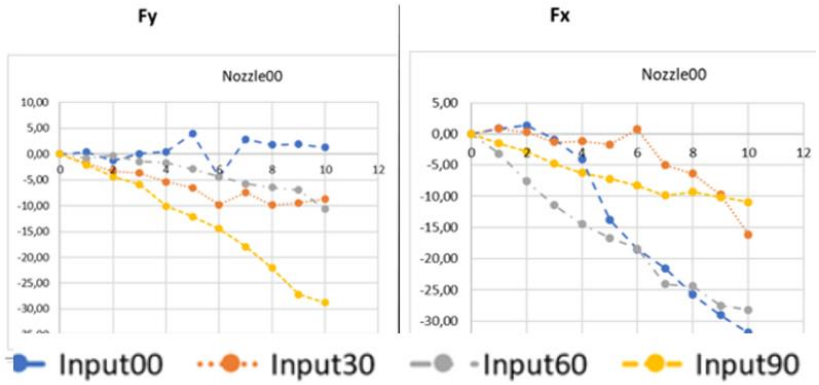

Figure 4.1 - Nozzle00 x axis force vs y axis force

4.2. Nozzle reaction expected forces (input and output angle variation)

Employing the theoretical model above-developed and the theoretical input velocity values [Table 3.2], the nozzle reactions expected forces results were calculated [table 4.1] (neglecting hose tension and exclusively for the 10-bar pressure):

Table 4.1 - Theoretical results

Nozzle Angle	Input Angle	0	30	60	90
0	F_x	-4,83	-4,44	-3,37	-1,91
	F_y	-0,46	1,03	2,46	3,47
45	F_x	-4,27	-3,88	-2,81	-1,35
	F_y	-1,91	-0,43	1,01	2,01
90	F_x	-2,93	-2,53	-1,46	0,00
	F_y	-3,01	-1,53	-0,09	0,91

As observed in the previous table, the higher theoretical value obtained was for the linear hose-nozzle geometry x axis reaction. Comparing to the experimental value, results a relative error of around 550%, which demonstrates the risk of neglecting hose tension. Also, might result as well, in predicted nozzle reactions with different directions that the experimental ones. Table 4.2 displays an example that demonstrates the extreme difference (in magnitude and direction) of experimental results and theoretical results (neglecting hose tension).

Table 4.2 - U-bend geometry experimental vs theoretical results

		Experimental Results	Theoretical Results
Nozzle Angle	Input Angle	90	90
90	F_x	19,31	0,00
	F_y	-40,63	0,91

Towards a safe and careful project design of the two above-mentioned firefighting technologies, hose tension should not be neglected.

4.3. 90-degrees Two-Outputs Nozzle Hose Tension Calculation

In order to proceed to the Hose Tension's estimation, the following calculations were developed.

Table 4.1 displays the extracted load cell's results for the reactions along the y axis:

Table 4.3 - Reactions along y axis

Pressure	0	1	2	3	4	5
Inclined Input	0	2,25	-4,59	-13,72	-15,77	-20,15
Vertical Input	0	2,95	-4,28	-13,49	-22,01	-31,49

At this stage and observing theoretical model developed in subchapter 2.1.2. is possible to conclude that hose tension is the only unknown variable, so placing equation (2.16) in order to simply calculate hose tension component along the y axis (regarding $\overrightarrow{R_y}$ is opposite of the load cell's obtained value):

$$T = (-\overrightarrow{R_y} - A_{In}p_{In} + \frac{A_{in}^2}{A_{out}}V_{in}^2 - \rho {V_{In}}^2 A_{In})\hat{n}_{In} \tag{4.3}$$

Two-outputs nozzle's case does not fit as well in the friction losses theoretical model; thus, our method is simply calculating the input velocity dividing the flow by the input area. The previous process results in the values displayed in table 4.2:

Table 4.4 - Velocities calculated

Pressure Bar	Inclined Input m/s	Vertical Input m/s
1	2,23	2,48
2	3,60	3,72
3	4,83	5,05
4	5,88	5,96
5	6,52	6,58

Now, calculating hose tension's component along the y axis for the 90-degrees Two-Outputs' case, employing equation (4.1) results in the values displayed in table 4.3:

Table 4.5 – Calculated Hose Tension

Pressure Bar	0	1	2	3	4	5
Inclined Output N	0,00	4,35	-0,64	-6,93	-12,28	-19,53
Vertical Output N	0,00	0,91	2,65	6,01	8,71	10,66

As observed in the previous results, hose position affects extremely the magnitude and direction of the hose tension's force. Additionally, hose tension does not present neglectable values.

However, was obtained a not-neglectable value for the z axis force and considering the water pressure force has no component in the horizontal plan and velocity vectors equals (no flow represented in this plan):

$$\sum \vec{F} = \vec{R} + \vec{T} = 0 \tag{4.4}$$

Concluding:

$$-\vec{R} = \vec{T} \tag{4.5}$$

So, was assumed that the load cell force obtained along the z axis direction, represent the hose forces component along this direction, which demonstrates that hose tension is not along the input flow either the output flow direction.

It follows, in Table 4.6, the obtained results for the z axis force:

Table 4.6 – Reactions along z axis

Pressure	0	1	2	3	4	5
Inclined Output	0,00	0,43	1,10	2,54	2,07	2,46
Vertical Output	0,00	-0,82	-1,24	-1,16	-1,28	-1,52

For 5-bar pressure inclined input:

$$T = 2{,}46\hat{z} - 19{,}53\hat{y}$$

For 5-bar pressure vertical input:

$$T = -1{,}52\hat{z} - 10{,}66\hat{y}$$

The previous results demonstrate that hose position has impact in the hose tension forces' magnitude and direction. Also, hose tension forces do not are purely directed along the input flow direction or the output flow direction. The previous process can be performed for all the experiments performed, since this report displays the necessary data.

5. CONCLUSIONS

5.1. State-of-Art contribution

As above-mentioned, exclusively Chin et al. (2017)[3] and Vera et al. (2018)[10] addressed the forces exerted by the hose to the Nozzle Reaction problem. However, their model is insufficient for most practical cases, including ours, since it relies on assuming a large set of conditions (inviscid flow, frictionless contact with the ground, …). Additionally, Chin et al. (2017)[3] model produces reactions in the output flow direction only, which contradicts our experimental results.

Therefore, as demonstrated by our experimental results, forces exerted by the hose are the key to understand and model the nozzle reaction (which are the forces that the drone and the water monitor will have to withstand).

The horizontal nozzle trial was the first approach in order to model the nozzle reactions, the main observation obtained was that the measured torques changed extremely depending on whether the hose was supported on the ground or on the nozzle's height support. The referred experiment's results demonstrate that the forces exerted by the hose have a not neglectable impact in the reaction forces measured by the load cell.

Varying the input and output flow angles, allowed to observe that a part of the measured nozzle reactions cannot be comprehended without analysing the forces and moments exerted by the hose. This experiment obtained values resulted in the conclusions of section 4.1 (Chin's theoretical model cannot be used in real-life situations), since Chin el al. (2017) modelled nozzle reaction forces along the output flow direction, which is not consistent with the input and output angle variation trial results. The referred experiment was also important to notice that the force exerted by the hose is not purely directed along the output flow direction or the input flow direction.

From the two-output nozzles experiments of section 3.4 the main observation was the high torques around the horizontal axis, since these values cannot be explained without the above-mentioned effect due to the hose inner inertial forces whom try to enforce the hose to the most linear geometry allowed.

Finding a satisfying relationship between pressure and flow rate that characterize the pressure losses within the circuit (hose and nozzle), was a result of a favourable matching of the one-output-nozzle's flow analysis and the developed theoretical model and was imperative in order to perform an analysis where the exerted forces and moments by the hose were the only unknown variable. Since, as above-mentioned, the referred losses are independent of the input and output flow angles, the model could be simplified, considering that a unique model suffices all the experiment's configurations.

The two-outputs-nozzle does not fit in the theoretical model, by reason that it was developed for the one-output-nozzle's case.

Comparing the theoretical model relative to experimental results highlighted the risk of neglecting hose forces, since it results in enormous relative errors when estimating theoretical nozzle reactions. The referred comparison allowed hose tension forces estimations as well.

Thus, the conclusion is that in order to better design the mentioned firefighting technologies, it is crucial to consider and characterize the hose forces, since these are not neglectable and can represent up to 100% of the total reactions in the nozzle support. In mobile devices with a hose attached, such as the drone, it becomes even more important to consider such forces as they will be amplified by the movement of the hose and its friction with the ground.

5.2. Future perspetives

To be able to explain the experimental data observed, further theoretical analysis must be performed. A full theoretical model should be developed, and it is proposed to use Continuum Fluids Mechanics theory to tackle the problem.

Also, would be interesting to validate theoretical the value that sums up the pressure losses within the hose-nozzle circuit, as develop an accurate theoretical pressure *versus* flow model, regarding the two-outputs-nozzle, which would allow researchers to computing the hose forces in these two-output nozzles with more precision.

Regarding this thesis work results, an article is currently being prepared.

BIBLIOGRAPHY

[1] M. Beighley and A. C. Hyde, “Portugal Wildfire Management in a New Era Assessing Fire Risks, Resources and Reforms,” 2018.

[2] “Portugal’s wildfire that broke a community - BBC News.” [Online]. Available: https://www.bbc.com/news/world-europe-44438505. [Accessed: 04-Sep-2019].

[3] S. K. Chin, G. Jomaas, and P. B. Sunderland, “Firefighter Nozzle Reaction,” *Fire Technol.*, vol. 53, no. 5, pp. 1907–1917, 2017.

[4] “Flight Control - DJI Mobile SDK Documentation.” [Online]. Available: https://developer.dji.com/mobile-sdk/documentation/introduction/flightController_concepts.html. [Accessed: 05-Sep-2019].

[5] J. W. Warren, “Forces acting on a hose [4],” *Phys. Educ.*, vol. 10, no. 4, pp. 327–328, 1975.

[6] F. Vera, R. Rivera, and C. Núñez, “Backward Reaction Force on a Fire Hose, Myth or Reality?,” *Fire Technol.*, vol. 51, no. 5, pp. 1023–1027, 2015.

[7] “How to Calculate Nozzle Reaction.” [Online]. Available: https://www.fs.fed.us/eng/pubs/html/02511318/02511318.htm. [Accessed: 30-Aug-2019].

[8] “MEASURING AND DEMONSTRATING NOZZLE REACTION - Fire Engineering.” [Online]. Available: https://www.fireengineering.com/articles/print/volume-159/issue-4/features/measuring-and-demonstrating-nozzle-reaction.html#gref. [Accessed: 31-Aug-2019].

[9] P. Grimwood, “Firefighting Nozzle Reaction HIGH-RISE FIREFIGHTING FIREFIGHTER’S GUIDE 3D WATER-FOG POSITIVE PRESSURE (PPV) US NAVY 3D FOG TESTS FLASHOVER TRAINING LINKS UK FIRE ENGINEERING 3D FOG FIRE CHIEF 3D FOG THERMAL IMAGES PUBLICATIONS STRATEGY & TACTICS AUSTRALIA FIRENET UK EUROPEAN LINKS TORE FAGERHOV FIREFIGHTING FLOW-RATES GREAT LINKS FDNY WTC TRIBUTE DOWNLOAD REPORTS KINGS CROSS FIRE 1987 NOZZLE TECHNIQUES FIRE MODELING TBA TBA TBA.”

[10] F. Vera, R. Rivera, and C. Núñez, “Backward Reaction Force in a Firehose,” *Fire Technol.*, vol. 54, no. 4, pp. 811–818, 2018.

[11] L. A. Oliveira and A. G. Lopes, *Mecânica dos Fluídos*, 4ª. Lidel, 2012.

ANNEX A

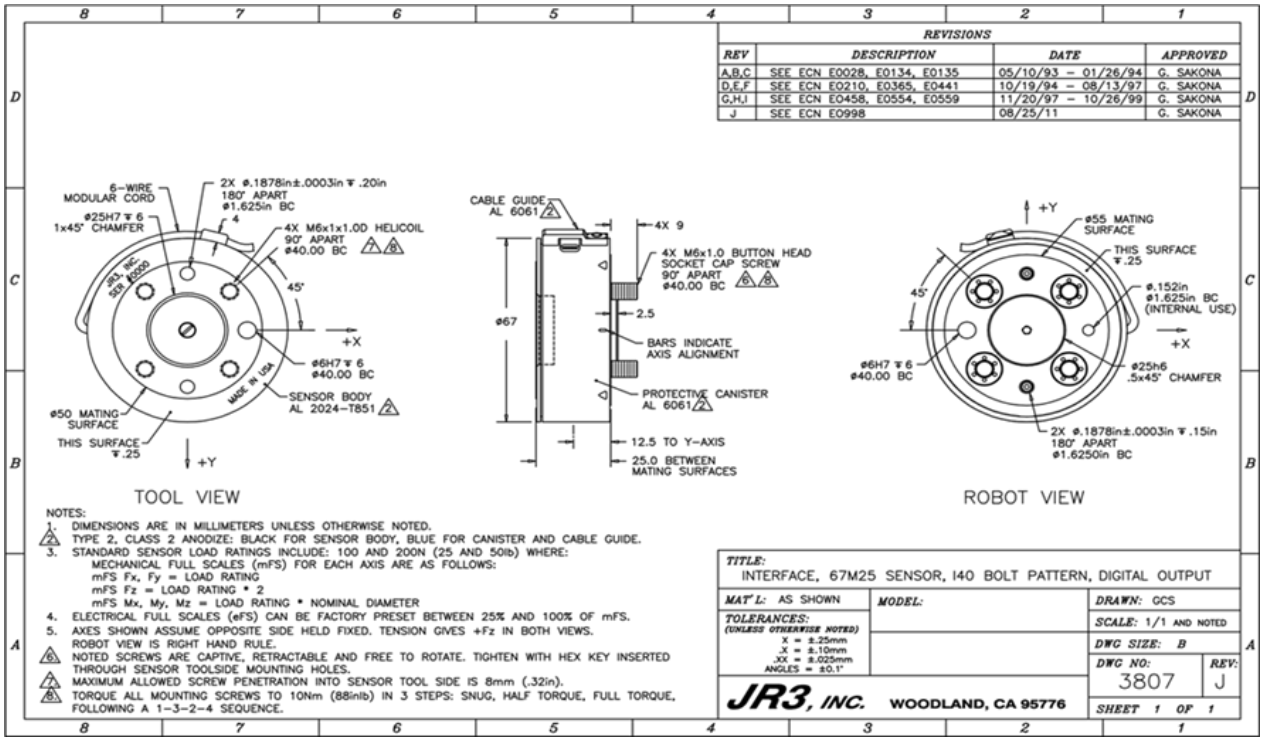

Figure 0.1 - 2D load cell draw

Table 0.1 - Calibration RAW data

Distance [mm]	Load [kg]	0	1	2	3	4	5
	Load [N]	0	9,81	19,62	29,43	39,24	49,05
	F_z	0	1198	2433	3643	4791	5990
	F_y	0	2502	5026	7453	9803	12274
	F_x	0	3400	6678	10119	13640	17175
	Moment [N.m]	0	0,4	0,8	1,3	1,7	2,1
42,5	M_z	0	1469	2888	4384	5904	7454
	Moment [N.m]	0	1,8	3,7	5,5	7,3	9,1
186,1	M_y	0	9249	17992	27017	32768	32769
	Moment [N.m]	0	1,8	3,7	5,5	7,3	9,2
186,7	M_x	0	9535	19240	28763	32765	32765

Table 0.2 - Horizontal nozzle trial forces results

	Pressure [bar]	0	1	2	3	4	5	6	7	8	9	10	Calibration	Maximums	Units
F_x	0-degrees	0,0	-1,1	-2,3	-8,2	-12,0	-16,4	-22,8	-26,7	-29,8	-34,0	-39,9	347,6	-39,9	N
	supported	0,0	1,7	-1,2	-6,0	-11,5	-15,3	-21,6	-24,6	-30,2	-36,2	-40,2	347,6	-40,2	N
	30-degrees	0,0	0,4	-1,0	-4,1	-12,1	-16,5	-18,5	-21,0	-24,7	-29,1	-31,8	347,6	-31,8	N
	60-degrees	0,0	-2,3	-4,1	-5,6	-8,8	-11,6	-12,3	-15,9	-18,5	-19,8	-21,3	347,6	-21,3	N
F_y	0-degrees	0,0	-0,7	-2,5	-2,8	-3,5	-4,0	-2,9	-4,0	-3,6	-4,0	-5,2	251,13	-5,2	N
	supported	0,0	0,1	-0,1	-0,5	-1,0	-1,0	-1,1	-1,5	-2,4	-3,3	-4,4	251,13	-4,4	N
	30-degrees	0,0	1,6	3,0	6,4	10,9	14,4	16,2	17,1	21,2	24,3	27,4	251,13	27,4	N
	60-degrees	0,0	2,9	7,6	9,9	16,5	19,3	22,1	25,9	31,0	30,0	40,2	251,13	40,2	N
F_z	0-degrees	0,0	-1,1	-1,2	-1,5	-1,2	-1,2	-1,9	-1,6	-2,5	-2,0	-1,0	122,52	-2,5	N
	supported	0,0	0,5	1,1	1,8	2,8	3,1	3,3	4,3	4,4	5,3	6,1	122,52	6,1	N
	30-degrees	0,0	-0,4	-0,5	0,2	1,7	2,1	3,2	2,3	3,5	4,3	6,0	122,52	6,0	N
	60-degrees	0,0	0,6	1,1	0,6	2,2	2,4	2,4	3,9	4,5	5,6	4,8	122,52	5,6	N

Table 0.3 - Horizontal nozzle trial moments results

	Pressure [bar]	0	1	2	3	4	5	6	7	8	9	10	Calibration	Maximums	Units
M_x	0-degrees	0,0	0,2	0,2	0,3	0,3	0,4	0,6	0,6	0,7	0,8	0,9	5237,8	0,9	**N.m**
	supported	0,0	0,1	0,2	0,2	0,3	0,3	0,3	0,4	0,4	0,5	0,5	5237,8	0,5	**N.m**
	30-degrees	0,0	0,1	0,1	0,2	0,2	0,2	0,3	0,2	0,4	0,5	0,7	5237,8	0,7	**N.m**
	60-degrees	0,0	0,1	0,3	0,4	0,7	0,9	1,0	1,2	1,4	1,5	1,8	5237,8	1,8	**N.m**
M_y	0-degrees	0,0	-0,1	-0,4	-0,6	-0,6	-0,6	-0,2	-0,3	-0,4	-0,3	-0,4	4940,6	-0,6	**N.m**
	supported	0,0	-0,3	-0,4	-0,3	-0,2	-0,1	0,0	0,1	0,1	0,2	0,3	4940,6	-0,4	**N.m**
	30-degrees	0,0	-0,1	-0,1	-0,1	-0,2	-0,4	-0,3	-0,5	-0,6	-0,5	-0,4	4940,6	-0,6	**N.m**
	60-degrees	0,0	0,0	0,0	0,0	0,0	0,0	0,0	0,0	0,0	0,0	-0,1	4940,6	-0,1	**N.m**
M_z	0-degrees	0,0	1,0	1,3	1,9	2,2	2,4	2,8	3,0	3,2	3,5	3,7	3544,7	3,7	**N.m**
	supported	0,0	0,1	-0,1	-0,3	-0,6	-0,8	-0,9	-1,1	-1,4	-1,7	-1,7	3544,7	-1,7	**N.m**
	30-degrees	0,0	0,3	0,3	0,2	-0,5	-0,7	-0,8	-0,9	-1,1	-1,3	-1,5	3544,7	-1,5	**N.m**
	60-degrees	0,0	-0,7	-1,2	-1,5	-2,1	-2,6	-2,9	-3,4	-4,1	-4,4	-4,8	3544,7	-4,8	**N.m**

Table 0.4 - Horizontal nozzle trial resultant forces

Resultant Force [N]											
Pressure	0	1	2	3	4	5	6	7	8	9	10
0-degrees	0,00	1,71	3,58	8,83	12,57	16,91	23,03	27,06	30,11	34,24	40,20
0-degrees supported	0,00	1,80	1,64	6,28	11,85	15,68	21,84	25,04	30,62	36,78	40,88
30-degrees	0,00	1,66	3,18	7,60	16,41	21,99	24,85	27,18	32,73	38,14	42,40
60-degrees	0,00	3,70	8,69	11,36	18,87	22,64	25,42	30,64	36,35	36,35	45,74

Table 0.5 - Input/output angle variantion results (0-degrees input angle)

	Input Angle 0 degrees											
Nozzle Angle	Pressure [bar]	0	1	2	3	4	5	6	7	8	9	10
0 degrees	F_x [N]	0,00	0,84	1,38	-0,88	-4,09	-13,81	-18,48	-21,54	-25,75	-29,07	-31,85
	F_y[N]	0,00	0,41	-1,29	0,05	0,46	3,95	-4,46	2,86	1,78	1,93	1,30
	F_z[N]	0,00	0,15	-1,31	-2,60	-2,95	-0,90	1,89	1,50	0,82	2,71	3,61
	M_x[N.m]	0,00	0,00	0,20	0,40	0,42	0,67	0,61	0,81	0,89	0,85	0,95
	M_y [N.m]	0,00	-0,11	-0,03	-0,17	-0,74	-1,15	-2,73	-2,55	-3,17	-3,41	-3,41
	M_z [N.m]	0,00	-0,13	0,95	1,73	2,42	2,84	3,22	3,43	3,56	3,64	3,77
45 degrees	F_x [N]	0,00	2,77	2,10	4,64	6,76	8,49	7,93	5,26	2,52	-0,35	-4,34
	F_y[N]	0,00	-5,19	-7,59	-14,00	-21,43	-25,77	-30,77	-32,41	-33,37	-38,09	-40,95
	F_z[N]	0,00	-0,67	-0,92	-0,97	-2,02	-1,30	-1,69	-3,53	-3,72	-5,15	-5,71
	M_x[N.m]	0,00	0,03	0,12	0,14	0,14	0,13	0,20	0,46	0,53	0,71	0,61
	M_y [N.m]	0,00	-0,18	-0,14	-0,37	-0,60	-0,82	-0,96	-0,83	-0,58	-0,38	-0,29
	M_z [N.m]	0,00	0,65	1,06	1,44	1,87	2,02	2,50	3,35	4,07	5,18	5,54
90 degrees	F_x [N]	0,00	-0,26	9,49	11,69	12,77	14,05	16,24	15,79	16,36	16,59	18,43
	F_y[N]	0,00	1,37	-7,70	-9,97	-11,89	-15,78	-18,76	-19,93	-22,22	-25,36	-29,68
	F_z[N]	0,00	-0,03	-1,06	-1,35	-1,28	-0,94	-0,98	-0,77	-0,05	-0,30	0,42
	M_x[N.m]	0,00	0,05	0,07	0,21	0,27	0,40	0,46	0,54	0,47	0,77	0,70
	M_y [N.m]	0,00	0,04	-1,07	-1,65	-2,01	-2,63	-3,00	-3,14	-3,43	-3,77	-4,10
	M_z [N.m]	0,00	0,13	1,73	2,50	3,02	4,07	4,72	4,89	5,20	6,06	6,61

Table 0.6 - Input/output angle variantion results (0-degrees input angle)

	Input Angle 30 degrees											
Nozzle Angle	Pressure [bar]	0	1	2	3	4	5	6	7	8	9	10
0 degrees	F_x [N]	0,000	0,877	0,316	-1,292	-1,191	-1,677	0,768	-4,983	-6,341	-9,741	-16,125
	F_y[N]	0,000	-1,824	-3,277	-3,687	-5,356	-6,519	-9,796	-7,426	-9,855	-9,469	-8,661
	F_z[N]	0,000	-0,743	-1,445	-1,567	-2,302	-3,542	-3,346	-3,640	-4,824	-3,738	-4,546
	M_x[N.m]	0,000	0,114	0,198	0,275	0,373	0,479	0,465	0,566	0,667	0,770	0,978
	M_y [N.m]	0,000	-0,061	-0,129	-0,021	-0,098	-0,309	-0,342	-0,370	-0,510	-0,274	-0,088
	M_z [N.m]	0,000	0,633	1,151	1,438	1,864	2,197	2,661	2,986	3,310	3,221	2,762
45 degrees	F_x [N]	0,000	1,979	3,395	4,051	6,220	9,100	9,882	8,196	4,071	-0,095	-6,959
	F_y[N]	0,000	-6,335	-13,714	-20,241	-25,963	-31,693	-40,015	-40,409	-40,987	-43,754	-44,798
	F_z[N]	0,000	-1,632	-3,550	-5,411	-6,587	-7,264	-10,455	-8,945	-6,840	-5,770	-3,828
	M_x[N.m]	0,000	-0,065	-0,135	-0,143	-0,159	-0,211	-0,253	-0,243	-0,410	-0,546	-0,509
	M_y [N.m]	0,000	-0,220	-0,433	-0,557	-0,832	-0,907	-1,128	-1,429	-1,689	-1,902	-1,963
	M_z [N.m]	0,000	0,381	0,858	1,386	1,633	2,003	2,241	2,611	2,372	2,002	1,978
90 degrees	F_x [N]	0,000	8,357	9,626	8,297	5,670	5,072	4,381	7,209	8,645	9,097	10,797
	F_y[N]	0,000	-6,132	-7,446	-8,338	-9,716	-11,683	-13,419	-17,294	-19,882	-24,139	-26,739
	F_z[N]	0,000	-1,363	-0,531	0,604	1,314	2,253	3,102	3,142	3,469	5,264	5,044
	M_x[N.m]	0,000	-0,103	-0,154	-0,204	-0,179	-0,244	-0,292	-0,338	-0,433	-0,608	-0,630
	M_y [N.m]	0,000	-0,377	-1,104	-1,594	-1,851	-2,218	-2,539	-3,011	-3,373	-4,039	-4,235
	M_z [N.m]	0,000	1,227	1,867	2,174	2,397	2,755	3,058	3,449	3,412	3,911	3,921

Table 0.7 - Input/output angle variantion results (0-degrees input angle)

Input Angle 60 degrees											
Pressure [bar]	0	1	2	3	4	5	6	7	8	9	10
F_x [N]	0,00	-3,12	-7,59	-11,44	-14,51	-16,71	-18,39	-24,06	-24,42	-27,52	-28,20
F_y[N]	0,00	-0,81	-0,32	-1,42	-1,70	-2,89	-4,35	-5,74	-6,45	-6,96	-10,62
F_z[N]	0,00	0,74	1,11	1,62	2,06	1,86	2,72	2,69	2,42	2,76	3,26
M_x[N.m]	0,00	-0,02	0,02	-0,01	0,00	-0,03	-0,02	-0,06	-0,07	-0,08	-0,15
M_y [N.m]	0,00	-0,03	0,00	0,02	-0,08	-0,19	-0,16	-0,25	-0,45	-0,39	-0,38
M_z [N.m]	0,00	-0,51	-1,02	-1,42	-1,70	-1,80	-2,02	-2,13	-2,21	-2,29	-2,29
F_x [N]	0,00	-0,75	-3,41	-5,25	-7,68	-8,06	-9,87	-10,91	-12,45	-11,76	-11,07
F_y[N]	0,00	-4,11	-6,98	-12,74	-17,37	-20,62	-25,50	-30,38	-36,17	-43,98	-51,45
F_z[N]	0,00	-0,07	0,91	0,80	0,73	0,87	0,46	-0,35	-0,24	-0,21	0,05
M_x[N.m]	0,00	-0,18	-0,39	-0,60	-0,72	-0,78	-0,98	-1,03	-1,10	-1,33	-1,55
M_y [N.m]	0,00	-0,21	-0,29	-0,48	-0,62	-0,72	-0,83	-1,00	-1,11	-1,27	-1,48
M_z [N.m]	0,00	-0,12	-0,51	-0,83	-0,99	-1,09	-1,16	-1,24	-1,18	-1,07	-1,08
F_x [N]	0,00	2,15	3,92	6,17	6,79	9,66	11,18	11,05	13,84	14,70	13,56
F_y[N]	0,00	-4,00	-7,64	-11,25	-14,78	-19,14	-22,09	-25,11	-28,23	-30,94	-34,09
F_z[N]	0,00	1,08	2,15	3,00	4,09	5,31	6,81	7,83	9,10	9,79	11,26
M_x[N.m]	0,00	-0,29	-0,58	-0,85	-1,11	-1,52	-1,78	-2,06	-2,39	-2,62	-2,81
M_y [N.m]	0,00	-0,31	-0,60	-0,93	-1,20	-1,64	-1,91	-2,21	-2,55	-2,79	-3,01
M_z [N.m]	0,00	-0,06	-0,06	0,02	-0,11	-0,06	-0,14	-0,50	-0,52	-0,55	-1,31

Table 0.8 - Input/output angle variantion results (0-degrees input angle)

	Input Angle 90 degrees											
Nozzle Angle	Pressure [bar]	0	1	2	3	4	5	6	7	8	9	10
0 degrees	F_x [N]	0,00	-1,52	-2,82	-4,80	-6,26	-7,21	-8,26	-9,87	-9,32	-10,15	-10,92
	F_y[N]	0,00	-2,10	-4,40	-5,89	-10,06	-12,09	-14,44	-17,95	-22,05	-27,20	-28,80
	F_z[N]	0,00	0,37	0,87	0,75	1,59	1,88	2,53	2,40	2,29	2,76	3,40
	M_x[N.m]	0,00	-0,29	-0,50	-0,64	-1,04	-1,28	-1,50	-1,90	-2,27	-2,63	-2,86
	M_y [N.m]	0,00	-0,16	-0,24	-0,38	-0,53	-0,70	-0,91	-1,10	-1,40	-1,51	-1,78
	M_z [N.m]	0,00	0,33	0,43	0,52	0,69	0,79	1,13	1,43	1,80	2,15	2,25
45 degrees	F_x [N]	0,00	1,39	0,97	1,05	0,58	1,45	1,60	2,25	2,25	2,81	5,41
	F_y[N]	0,00	-10,78	-16,37	-19,55	-26,72	-35,74	-41,53	-52,43	-59,89	-69,82	-79,04
	F_z[N]	0,00	-0,66	-0,95	-0,74	-0,42	-1,07	-1,49	-1,96	-2,57	-2,65	-3,81
	M_x[N.m]	0,00	-0,41	-0,70	-0,90	-1,20	-1,45	-1,61	-1,89	-2,17	-2,56	-2,63
	M_y [N.m]	0,00	-0,27	-0,50	-0,65	-0,78	-1,06	-1,26	-1,37	-1,61	-1,86	-2,25
	M_z [N.m]	0,00	0,43	1,06	1,48	1,90	2,47	2,94	3,49	3,90	4,63	5,05
90 degrees	F_x [N]	0,00	4,62	8,50	12,92	12,43	15,90	15,98	18,46	19,59	18,21	19,31
	F_y[N]	0,00	-4,84	-9,60	-15,20	-17,36	-22,43	-25,55	-30,68	-33,81	-35,71	-40,63
	F_z[N]	0,00	-0,73	-1,32	-1,90	-0,13	0,38	1,46	2,81	3,10	4,55	5,31
	M_x[N.m]	0,00	-0,12	-0,30	-0,43	-0,74	-0,98	-1,20	-1,55	-1,73	-1,93	-2,19
	M_y [N.m]	0,00	-0,28	-0,55	-0,87	-1,04	-1,29	-1,42	-1,70	-1,85	-1,90	-2,11
	M_z [N.m]	0,00	1,06	1,87	2,74	1,62	1,65	0,92	0,21	0,10	-0,95	-1,56

Table 0.9 – Two-outputs trial average results

Nozzle	Pressure	1	2	3	4	5
90-degrees Vertical Input	F_x [N]	-0,43	-1,18	-1,53	-2,01	-1,62
	F_y[N]	2,25	-4,59	-13,72	-15,77	-20,15
	F_z[N]	0,43	1,10	2,54	2,07	2,46
	M_x[N.m]	-0,04	-0,60	-1,22	-1,18	-1,37
	M_y [N.m]	0,03	0,06	0,03	0,03	0,24
	M_z [N.m]	-0,09	-0,20	-0,19	-0,40	-0,34
90-degrees Inclined Input	F_x [N]	0,16	0,10	-0,23	-0,32	-0,96
	F_y[N]	2,95	-4,28	-13,49	-22,01	-31,49
	F_z[N]	-0,82	-1,24	-1,16	-1,28	-1,52
	M_x[N.m]	0,19	-0,02	-0,41	-0,70	-1,10
	M_y [N.m]	-0,02	0,00	-0,01	0,04	0,18
	M_z [N.m]	0,47	0,74	0,78	1,00	1,06
45-degrees	F_x [N]	0,37	0,17	0,59	1,41	
	F_y[N]	3,74	-3,75	-11,58	-19,77	
	F_z[N]	0,80	2,68	3,37	5,04	
	M_x[N.m]	-0,18	-0,78	-1,40	-2,10	
	M_y [N.m]	-0,03	-0,10	-0,19	-0,52	
	M_z [N.m]	0,10	-0,10	0,00	0,20	

Table 0.10 - Friction loss trial results

Flow (litres per minute)													
Pressure (bar)	Test 1	Test 2	Test 3	Test 4	Test 5	Average	Test 6	Test 7	Test 8	Test 9	Test 10	Average	Theoretical Values (K=210)
1	20,93	19,74	23,6	20,13	30,8	23,04	18,47	23,96	21,88	33,39	33,1	26,16	21,00470
2	35,44	32,1	36,5	35,37	39,02	35,686	36,32	36,46	37,26	40,29	40,16	38,098	29,70514
3	39,49	39,19	38,55	40,63	39,1	39,392	37,07	35,52	38,05	41,7	45,75	39,618	36,38121
4	42,56	40,49	41,48	46,19	40,46	42,236	39,27	40,56	39,29	49,35	56,04	44,902	42,00941
5	44,12	45,71	44,46	45,59	42,56	44,488	41,6	41,94	40,51	58,51	56,6	47,832	46,96794
6	46,49	49,75	49,13	47,6	53,36	49,266	45,35	50,64	49,27	57,06	60,56	52,576	51,45081
7	49,62	52,94	51,04	58,52	56,51	53,726	50,21	50,62	50,96	67,07	72,37	58,246	55,57322
8	63,23	56,61	62,91	57,37	55,23	59,07	59,17	51,65	52,23	69,08	72,64	60,954	59,41027
9	62,99	64,52	63,11	58,24	57,85	61,342	60,56	54,61	55,02	69,81	73,66	62,732	63,01411
10	64,32	65,02	64,18	62,55	61,5	63,514	63,16	63,8	60,17	70,86	82,08	68,014	66,42270
Assembly	Input 0 degrees; Output 0 degrees						Input 90 degrees; Output 0 degrees						
Area	0,000506707 m^2												
K = k.g	210												